June 1998 • NREL/SR-520-24842

Optimization of Laser Scribing for Thin-Film PV Modules

Final Technical Progress Report 12 April 1995 - 11 October 1997

A.D. Compaan, I. Matulionis, and S. Nakade
The University of Toledo
Toledo, Ohio

National Renewable Energy Laboratory
1617 Cole Boulevard
Golden, Colorado 80401-3393
A national laboratory of the U.S. Department of Energy
Managed by Midwest Research Institute
for the U.S. Department of Energy
under contract No. DE-AC36-83CH10093

NREL/SR-520-24842

Optimization of Laser Scribing for Thin-Film PV Modules

Final Technical Progress Report 12 April 1995 - 11 October 1997

A.D. Compaan, I. Matulionis, and S. Nakade
The University of Toledo
Toledo, Ohio

NREL technical monitor: B. von Roedern

National Renewable Energy Laboratory
1617 Cole Boulevard
Golden, Colorado 80401-3393
A national laboratory of the U.S. Department of Energy
Managed by Midwest Research Institute
for the U.S. Department of Energy
under contract No. DE-AC36-83CH10093

Prepared under Subcontract No. ZAF-5-14142-08

June 1998

This publication was reproduced from the best available copy
Submitted by the subcontractor and received no editorial review at NREL

NOTICE

This report was prepared as an account of work sponsored by an agency of the United States government. Neither the United States government nor any agency thereof, nor any of their employees, makes any warranty, express or implied, or assumes any legal liability or responsibility for the accuracy, completeness, or usefulness of any information, apparatus, product, or process disclosed, or represents that its use would not infringe privately owned rights. Reference herein to any specific commercial product, process, or service by trade name, trademark, manufacturer, or otherwise does not necessarily constitute or imply its endorsement, recommendation, or favoring by the United States government or any agency thereof. The views and opinions of authors expressed herein do not necessarily state or reflect those of the United States government or any agency thereof.

Printed on paper containing at least 50% wastepaper, including 10% postconsumer waste

Summary

This report covers the final eighteen months of a project which was planned for 24 months but was given a six-month no-cost extension for a total of 30 months. The project goals included the investigation of several different types of lasers for scribing of materials used for polycrystalline thin-film photovoltaics. The materials investigated included the semiconductors (cadmium telluride, copper indium gallium diselenide, and silicon), the transparent conducting oxides (fluorine-doped tin oxide and aluminum-doped zinc oxide), and the metals (molybdenum and gold). The laser systems are all commercially available and were chosen for the range of pulse durations and wavelengths available. We used two continuous-lamp-pumped, Q-switched Nd:YAG lasers with a wavelengths of λ=1064 nm and 532 nm, a flashlamp-pumped-Nd:YAG laser (λ=532 or 1064 nm), a copper-vapor laser (λ=511 and 578 nm), an XeCl-excimer laser (λ=308 nm), a KrF-excimer laser (λ= 248 nm) and a diode-laser-pumped Nd:YAG. In addition to the different wavelengths, these systems were chosen for the range of pulse durations available. The pulse durations range from 70- 600 nsec for the cw/Q-switched YAG, 55 nsec for the Cu-vapor, ~20 nsec for the excimers, 10 nsec for the flashlamp-pumped, Q-switched YAG, and down to 0.1 ns for the mode-locked Nd:YAG.

In general we find that the Q-switched, continuously-pumped Nd:YAG lasers either at 1064 nm or frequency-doubled at 532 nm give good results for most of the thin film materials. The most significant exception, of the materials studied, is ZnO:Al, which we were unable to scribe cleanly with visible or infrared wavelengths. Remarkably, the other transparent conducting oxide, SnO_2:F scribes cleanly at both YAG laser wavelengths although the threshold is high. The diode-pumped Nd:YAG laser represents a further improvement in compactness and reliability. The excimer lasers, XeCl and KrF, worked well for all materials including the transparent conducting oxides. However, these UV lasers, although they have low thresholds for scribing, appear to be limited in the maximum rate of removal per pulse. On the other hand, with their large energy per pulse, the excimer beams can be delivered to the film in a long line image which may allow scribing across an entire panel width without beam scanning.

Almost all of our studies were focused on film-side scribing, however, in the case of thicker films, ~15 μm or more, we have found better results for glass-side scribing. Some preliminary studies were made of interconnection scribes to examine issues related to electrical isolation and shunting. The ZnO:Al on CIGS was found to be the most difficult to obtain good electrical isolation with the best results obtained from excimer laser scribes.

Table of Contents

List of Figures

List of Tables

Introduction and Objectives

One of the most important aspects in moving from the cell level to the integrated module level in thin-film photovoltaics is to achieve reliable and reproducible cell interconnects having low series resistance and high shunt resistance, and to do this with a minimum of dead area between cells. It is known that mechanical scribing often produces considerable damage (*e.g.*, film tearing) surrounding the scribe. Laser scribing has shown the potential for superior scribe widths and profiles for many of the materials involved with thin-film PV. However, problems are also known to occur with a heat-affected zone around the scribe, and for some materials and some focus conditions, high positive ridges or "collars" are left along the scribe line. In addition, melt phase residue at the bottom of a scribe may potentially lead to a highly conductive phase which could introduce electrical shorts.

The commercially-available scribing systems have been optimized typically for other applications and other materials such as scribing of crystalline Si[1]. Optimum operation for thin-film PV materials has been investigated by several PV manufacturers[2,3,4] but there has been limited discussion of problems or of optimum parameters in the open literature. Furthermore, to our knowledge, there has been a limited number of reports of the application, for thin-film PV, of laser systems other than the traditional cw lamp-pumped, Q-switched Nd:YAG. Excimer lasers have been tested for a-Si:H[5] and for II-VI materials[6] and a continuous (non-pulsed) YAG beam has been tested on CIS [7]. To our knowledge the first U.S. patent for laser scribing for solar module integration was granted to J.J. Hanak in 1981[8]. Since then, a number of refinements of this method have been patented[9], mostly emphasizing a-Si:H and SnO_2, with at least one of these emphasizing the use of excimer lasers.

This two-year project was designed to improve our fundamental understanding of the laser scribing process and the role of the variables of laser wavelength, laser pulse duration, and pulse energy density on the quality, speed, and efficiency of scribing of thin-film PV materials. The materials under investigation include three semiconductors--cadmium telluride, copper indium gallium diselenide, and silicon, two transparent conducting oxides--fluorine-doped tin oxide and aluminum-doped zinc oxide, and two metals--molybdenum and gold. The laser systems are all commercial systems and were chosen for the range of pulse durations and wavelengths available. We have studied seven different laser systems, with wavelengths and pulse durations given in brackets -- the flashlamp-pumped Nd:YAG laser (fp-YAG) [λ=532 & 1064 nm, τ_p=10 nsec], the continuous-lamp-pumped and Q-switched Nd:YAG laser (cw-pulsed or cwp-YAG) [532/1064 nm, 90-600 nsec], the copper-vapor laser [511/578 nm, 50 nsec], the XeCl excimer laser [308 nm, 15 nsec], the KrF excimer laser [248 nm, 25 nsec], and, for the shortest pulse durations, we have used a cw-pumped, mode-locked Nd-YAG (cwp/ml-YAG) [1064/532 nm, 0.1 nsec]. Finally, we have tested a diode-laser-pumped Nd:YAG (dlp-YAG) [1064/532 mm, 70 ns].

In this final project report we shall, for completeness, summarize some of the results described in the first-year report, and provide a complete survey of results from all of the lasers tested and for all of the thin-film materials tested.

Laser Characteristics

The seven lasers studied in this project have pulse durations ranging from 600 nsec to 0.1 nsec. The wavelengths range from 1064 nm to 248 nm. At the longest wavelength of 1064 nm, all of the thin-film PV materials studied except molybdenum, gold, and copper indium gallium diselenide (CIGS) are transparent or nearly transparent. At the shortest wavelengths, all the thin-film materials studied here are strongly absorbing. In the following, we discuss the characteristics of each of the lasers individually, highlighting the differences among them. We want to emphasize here that not all of the lasers we have

used represent state-of-the-manufacturers-art and in some cases the output specifications are well below those which are available today. For example, our flashlamp-pumped Nd:YAG system discussed below is a vintage ~1980 system and the manufacturer of our 1988 excimer laser is no longer in business. Nevertheless, the critical parameters of pulse duration and wavelength have not changed. Presently available systems typically have improved beam quality, better pulse-to-pulse stability, and higher repetition rates. High pulse energy excimer lasers are available with repetition rates to 500 Hz and diode-laser-pumped YAG lasers are available combining compact heads and high operating efficiency.

The Nd:YAG Lasers

The Nd:YAG laser is the most commonly used type of laser for commercial laser scribing systems. The "YAG"(yttrium aluminum garnet) laser is available in a variety of configurations which also may utilize Nd in a host such as Nd:vanadate. The YAG is an optically pumped, doped ion (solid state) laser system with output characteristics which depend on the pump wavelength and intensity. In this work we used four different YAG systems: a flashlamp-pumped Nd:YAG (fp-YAG), a CW-lamp-pumped-Q-switched pulsed YAG (cwp-YAG), a CW-lamp-pumped-Q-switched-mode-locked YAG (cwp/ml-YAG), and a diode-laser-pumped-Q-switched YAG (dlp-YAG).

Flashlamp-pumped Nd:YAG--We used the flashlamp-pumped Nd:YAG (Quanta-ray DCR1-A) in the free-running mode (non-Q-switched) which typically yields several pulses with durations of ~190 to 400 nsec, depending on flashlamp energy. (Higher flashlamp energy yields shorter pulses.) Unfortunately pulse amplitude in the pulse train is quite variable. We also used this laser in the Q-switched mode in which an intracavity Q-switch holds off lasing during the flashlamp pulse until much higher population inversion is achieved. Then when the Q-switch "opens," a much higher pulse intensity and much shorter pulse duration occurs (10 ns at 1064 nm and 8 ns at 532 ns).

The fp-YAG laser has very high pulse energy but is not well suited to scribing because the repetition rates are typically limited to about 50 Hz due to heating in the YAG rod. Nevertheless, we used this laser to test scribing results at shorter pulse durations. Also the pulse characteristics illustrate very nicely the extremes related to the optical pumping conditions in the other YAG systems. This system, even without the use of the amplifier stage, has very high pulse energy, typically 100 mJ/pulse in the Q-switched mode at 1064 nm. Thus, in the present studies with spherical focussing, we have used substantial attenuation of this beam. The unstable resonator optics of this system do not give clean focal spot profiles without substantial aperturing. This laser, by virtue of its short pulse durations (~10 ns), provides an important comparison with the cwp-YAG system with pulses of 70-600 ns. As with most of the lasers, we observed the pulse shape with a p-i-n photodiode and a Hewlett-Packard model 54510A 1 Gsample/sec digitizing scope. The hard copy of the pulse shape was obtained via the HPIB interface to a personal computer.

Figure 1 shows that, when the laser is operated in the "free-running" mode, it emits trains of pulses (relaxation oscillations) with about a half dozen spikes near threshold to more than 50 at a flashlamp energy of 1.7 times threshold. These pulses are spread over a duration of about 50 μs near threshold to about 150 μs at the highest lamp energy. As shown in the inset to Fig. 1, the laser in this free running mode has individual pulse durations ranging from about 190 nsec to about 400 nsec depending on the flashlamp energy. The longest pulses occur at 33 J of lamp energy, very near the lasing threshold of 32 J. As the optical excitation increases and the gain increases, the pulse duration shortens considerably, down to 190 nsec.

When Q-switching is used in the flashlamp-pumped Nd:YAG, lasing is held off as the Pockels cell spoils the gain (increases the resonator loss) in the laser cavity and much higher population inversion is produced

in the laser rod until the resonator loss is rapidly switched low (on a time scale of 1 nsec--much less than the photon round trip time in the resonator). In this case the output pulse duration is very short, with the energy coupled out of the laser rod within 2 to 3 photon round trips in the resonator. The Q-switched pulse durations of both the fundamental wavelength (1064 nm) and the frequency-doubled wavelength (532 nm) are shown in Figures 2 & 3. We find pulse durations of 11 nsec and 8 nsec, respectively, for the fundamental and frequency-doubled outputs. The frequency-doubled pulse is slightly shorter in duration than the fundamental as a consequence of the nonlinear doubling process. There is some irregularity in the pulse shape which arises from beating of different longitudinal cavity resonances. Newer laser systems do not show these features, but we believe that they do not affect our scribing results in any case.

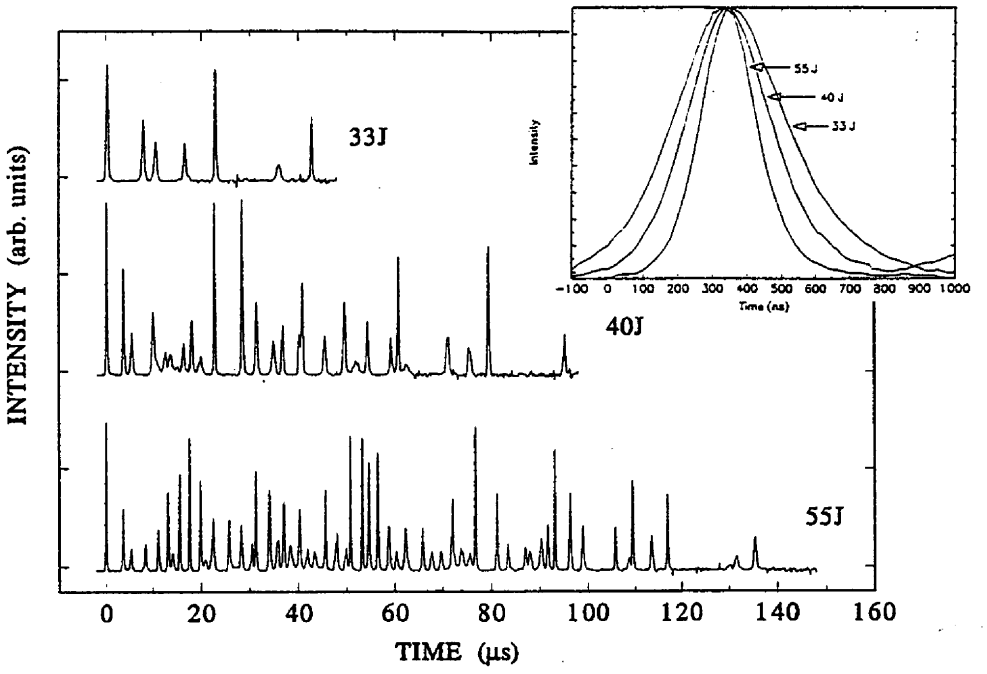

Fig. 1. Non-Q-switched output from FLP Nd:YAG laser showing spiking behavior for three different flashlamp energies. Note that the time scales are different for each trace. Inset shows a typical lasing spike at the various pump energies.

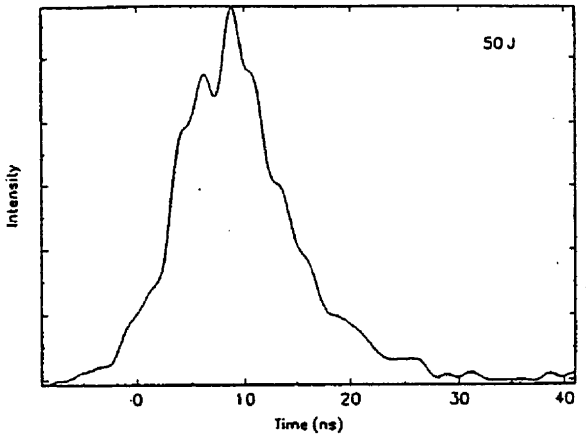

Fig.2. Temporal pulse profile of Q-switched FLP Nd:YAG at 1064 nm.

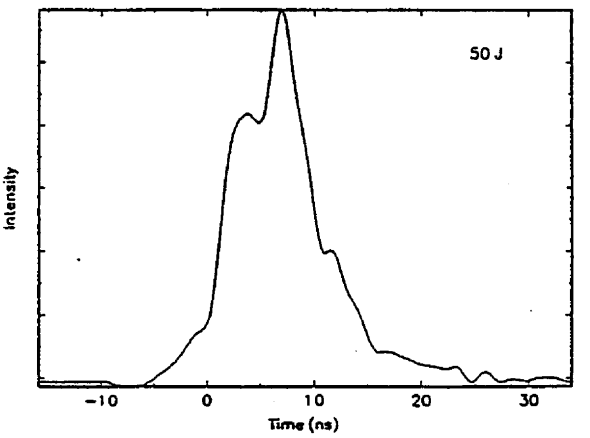

Fig. 3. Temporal pulse profile of Q-switched FLP Nd:YAG at 532 nm.

Much higher repetition rates are available from continuous-wave (CW) pumped and Q-switched Nd:YAG lasers. In our studies we used three different cw-pumped, Q-switched YAG lasers: a Kr-lamp-pumped, Q-switched laser (U.S. Laser model 403PQ), a Kr-lamp-pumped, Q-switched and mode-locked laser (Quantronix model 416) operated at both 1064 and 532 nm, and a diode-laser-pumped system (Spectra-Physics T40-X30-53QA).

The CW-pumped, Q-switched YAG--The U. S. Laser model 403PQ was used at Solar Cells Inc. (SCI) [10]. We shall refer to this system as the "cw-pulsed" or cwp-Nd:YAG system. It is sometimes called the "quasi-cw-YAG." We used this system in the frequency-doubled mode only. In the case of the cwp-YAG laser, the pulse temporal profile is very smooth but the width does depend on the repetition frequency. This is a consequence of the fact that with the continuous pumping of the Nd:YAG rod by the Kr lamp, the degree of population inversion attained by the time the intracavity Q-switch opens is larger for the low repetition rates. Consequently the photon density in the resonator rises more quickly when the Q-switch opens and drives the population inversion more quickly below threshold, leading to a shorter pulse duration. For the work reported here, the cwp-YAG laser was operated at a pulse repetition frequency (PRF) of 1 kHz in the frequency doubled mode where the pulse duration was 90 nsec with a tail which extended to about 150 nsec after the pulse peak. See Fig. 4. At 5 kHz the average power was about 2 W or 0.4 mJ/pulse in a single TEM_{00} mode.

SCI has provided us with their measurement of the relationship of the pulse duration to the repetition rate. This is shown in Fig. 5. Note that the pulse duration can range from 90 nsec at the lowest PRF (1 kHz) to ~600 nsec at 30 kHz.

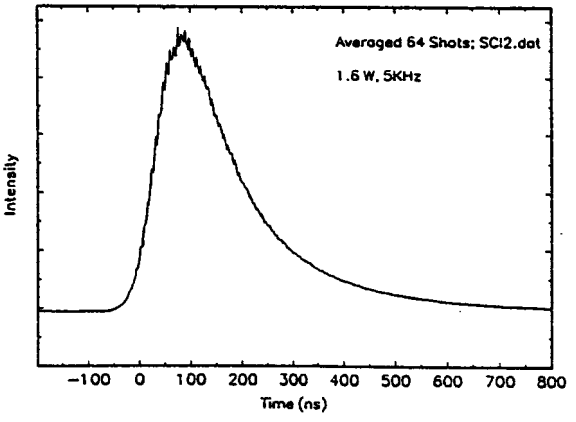

Fig. 4. Temporal pulse shape of cwp Nd:YAG at 5 kHz and 532 nm.

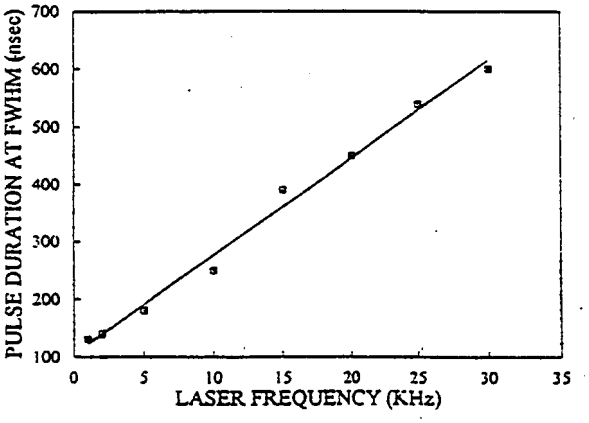

Fig. 5. Pulse duration vs. PRF for cwp Nd:YAG.

The CW-pumped, Q-switched, and mode-locked YAG--The Quantronix model 416 MLQsSH mode-locked and Q-switched Nd:YAG laser (cwp/ml-YAG) also is pumped by a cw Kr-lamp. Except for the mode-locking, this laser is similar to the cwp-YAG we have used at Solar Cells Inc which had 90 ns Q-switched pulses at 1 kHz. The Quantronix system has lower optical gain so that it produces longer Q-switched pulses (250 ns width at half-maximum) at 500 Hz, but it has the capability of mode-locking which yields a 250 ns long train of pulses each 0.1 ns in duration, spaced by about 15 ns, the laser resonator round-trip time. The laser resonator is extended to facilitate mode-locking. Digitized oscilloscope traces of these Q-switched-only and Q-switched-with-mode-locking pulses are shown in Fig. 6 for the 1064 nm and in Fig. 7 for the 532 nm, frequency-doubled case.

It should be noted that the pulse waveform with the modelocker turned off (Q-switched only) is actually partially modelocked in the fundamental (Fig. 6 b) and quite strongly modelocked in the case of the frequency doubled output (Fig. 7 b). This partial modelocking even with active mode-locking turned off, leads to some difficulty in interpretation of the scribing results discussed below. However, the scribing results are probably more strongly affected by the fact that the picosecond pulses are only available in a train of many pulses separated by about 15 ns, which is too little time for thermal diffusion between individual picosecond pulses so that the results are very similar to the non-mode-locked results. Modelocking does increase the peak *power* substantially--by the ratio of mode-locked pulse duration (~0.1 ns) to the separation between pulses, or 15ns/0.1ns = 150. However, we have not observed effects which we could clearly identify with the higher instantaneous peak power.

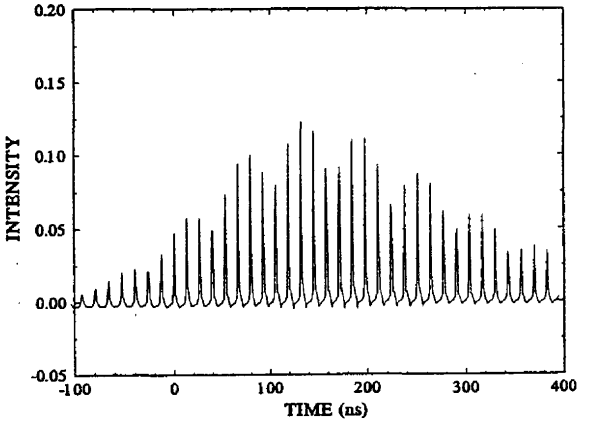

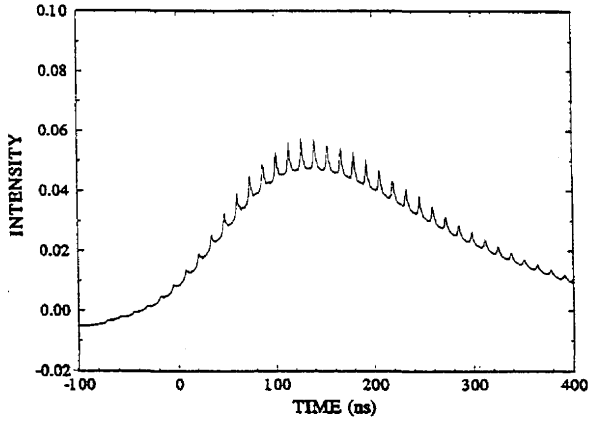

Fig. 6. Digitized oscilloscope traces of typical a) modelocked/Q-switched and b) Q-switched only pulses at 1064 nm. Note that at 100 ns per division, the apparent fluctuation of adjacent pulse heights is an artifact of the oscilloscope sampling rate.

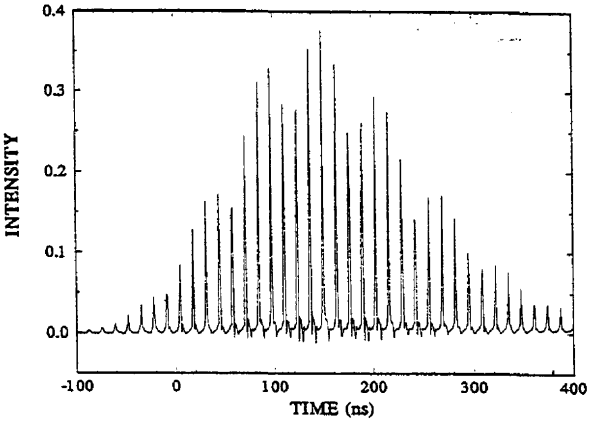

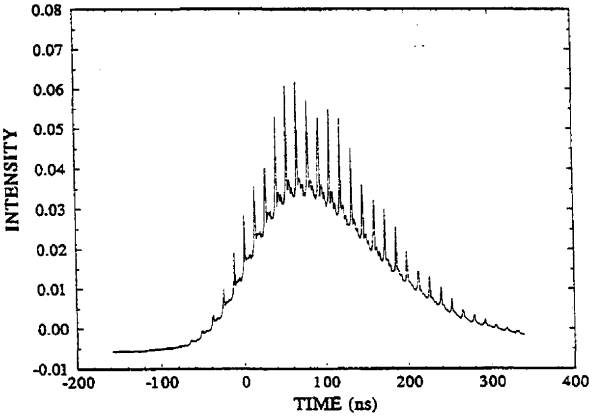

Fig. 7. Digitized traces of a) modelocked/Q-switched and b) Q-switched only pulses at 532 nm.

The diode-laser-pumped Nd:YAG--The CW diode laser pumping takes advantage of a much closer optical wavelength match to the output YAG wavelength so that less heat is dissipated in the YAG rod. This leads to less thermal lensing and smaller laser head size. In addition, the better coupling between pump and Nd ions permits high repetition rates with shorter pulse durations than for the lamp-pumped systems. Thus the Spectra Physics T40-Y70-106Q system (referred to here as dlp-YAG) has a nominal pulse duration of 70 ns at 1064 nm. The pulse shape is qualitatively similar to that shown in Fig. 4 above with a fast-rising leading edge and a longer trailing edge. Similar to the CW lamp-pumped YAG (Fig. 5, above), the pulse duration increases as the pulse repetition frequency (PRF) increases. For this diode-pumped system, the pulse width at about 1 kHz or less is 60-70 ns, increases to about 130 ns at 10 kHz and ~200 ns at 20 kHz. The pulse energy at 1 kHz is rated at 1.5 mJ. As the PRF increases, the individual pulse energy decreases for repetition rates above about 2 kHz. This behavior needs to be kept in mind if the highest PRFs are used. The average power is nearly constant at 7W for PRFs above about 10 kHz. This system is available with a frequency doubler to operate at 532 nm. Because of the quadratic dependence of the doubled intensity on the fundamental intensity, the average power at the doubled frequency reaches a maximum at about 7 kHz. The pulse energy in the green at 1 kHz is 1 mJ.

In this system, the pump laser diodes are fiber-optically coupled to the head which is much smaller than any of the other laser systems tested. In addition the diode pumping promises high reliability and low maintenance. Because of the end pumping of the YAG rod, the mode quality is TEM_{00} with a beam divergence of 1.2 mr. This is a particularly convenient system to use. Our scribing studies with this system were carried out in the Spectra Physics applications laboratory in Mountain View, Calif. [11].

The Copper-Vapor Laser

Our most recent studies of this laser for scribing applications were carried out at the University of Dayton Research Institute. The copper-vapor laser (CJL model MVL-2210) has output transitions at 510.6 nm and 578 nm (green and yellow) with about 25 % of the 16 watts of power appearing in the yellow transition. Since the pulse repetition frequency was 8 kHz, the energy per pulse was 2 mJ. In order to simplify analysis of the coupling to the various materials and to simplify our attenuation system, which used a rotatable dielectric filter, we used a dichroic filter to eliminate the 25% of the energy which appeared at 578 nm.

A plot of the pulse shape is given in Fig. 8. The full width at half maximum is 57 nsec. The pulse trace is very reproducible and shows some regular oscillation within the pulse envelope. These oscillations probably arise from rf pick-up although there may be some contribution from the beating of longitudinal modes in this system with resonator length of 96 inches (246 cm). The Fabry-Perot resonances in a resonator of this length would yield a longitudinal mode spacing of $\Delta\nu = c/2L = 60$ GHz. The beat period of adjacent longitudinal modes would be $T = 1/\Delta\nu =$ 16 nsec, very close to the observed oscillations. Note that there is essentially no tail of the lasing pulse beyond two half-widths from the pulse peak.

The laser we used had an extended cavity design with unstable resonator optics. These optics provide a beam of about 20 mm diameter and a very low beam divergence of 0.1 mrad. Using a 100 mm focal length lens, we easily achieved scribe linewidths of 50 to 150 μm. This laser depends on the longitudinal discharge for vaporizing the copper metal which lies in resevoirs at the bottom of the laser tube/discharge channel. Consequently it has a long warm-up time (≥ 1 hr) and can only be operated in the horizontal position. These, and the need for periodic metal recharge, would be concerns in a manufacturing environment. However, this laser does have a very high repetition rate (12 kHz) and short pulse durations (~50 ns).

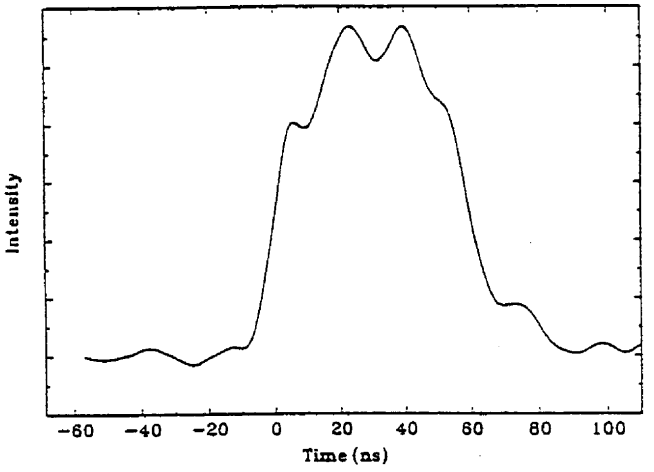

Fig. 8. Temporal profile of the copper-vapor laser pulse at 8 kHz.

The Excimer Lasers

There are several differences between the excimer lasers and the other laser systems in this study. The excimers are transverse discharge lasers with very high gain so that with standard plane-parallel mirrors (marginally stable resonator), the transverse mode quality is poor. In addition, the transverse discharge does not naturally produce an axially-symmetric beam. However, the pulse energies are very high so that, with some attention to beam shaping, beam homogenization, and the use of cylindrical focussing, it is possible to consider delivering to the film a line image which covers the entire module width. This could obviate the need for beam scanning and also permit active adjustment of the pulse energy as the scribe depth reaches an interface, e.g., CdTe on SnO_2 or CIGS on Mo.

The XeCl excimer--For the Questek model 2240 with a gas fill for XeCl, we typically run with a pulse energy of 80 mJ and repetition rates <30 Hz, although the system is designed for 200 Hz. Because of the high pulse energy and the poor beam quality of this laser we have typically used considerable attenuation and aperturing of the beam. We observe a beam divergence in the horizontal and vertical directions of 10 mrad and 2 mrad respectively. Using a spherical lens the focal spot from our laser is approximately a rectangle and, with moderate aperturing, can produce a very fine line. Actually, we have found it most convenient to use cylindrical focussing for this type of beam. The temporal pulse profile of the XeCl excimer laser is shown in Fig. 9. The pulse profile exhibits a full width at half maximum of 20 nsec with a slight tail trailing to longer times. We are using He as the buffer gas in this laser which yields a slightly shorter pulse duration than Ne as a buffer gas but also a slightly lower pulse energy.

The KrF excimer--The model LPX200 KrF laser was used in the applications facility of Lambda Physik in Fort Lauderdale, FL [12]. The 248 nm wavelength of the KrF yields a photon energy of 5.00 eV which is significantly higher than the 4.03 eV photon energy of the XeCl laser at $\lambda = 308$ nm. Actually the increased photon energy is not a major factor because 4 eV is already above the band gap energies for all of the PV materials of interest. The KrF laser at Lambda Physik had much better beam quality than our 1988-vintage Questek XeCl. This excimer is available in a version with 500 mJ per pulse and PRF to 500 Hz. In addition, we had available a beam homogenization system with optical imaging from a mask plane to the workpiece plane. This allowed us to test the concept of imaging to a long line, even though the Microlas imaging system [13], used typically for marking operations, was far from optimum for laser scribing. Only a small fraction of the beam energy was imaged onto the film in our tests. For example, most of our data were obtained with the homogenizer producing a very uniform 14 x 14 mm beam on a slit mask (20 mm x 0.27 mm) so that only about 0.27mm/14mm = 2% of the pulse energy was delivered to the film plane. The imaging system produced a (de)magnification of 1/4.5 so that the scribe width was ~60 μm.

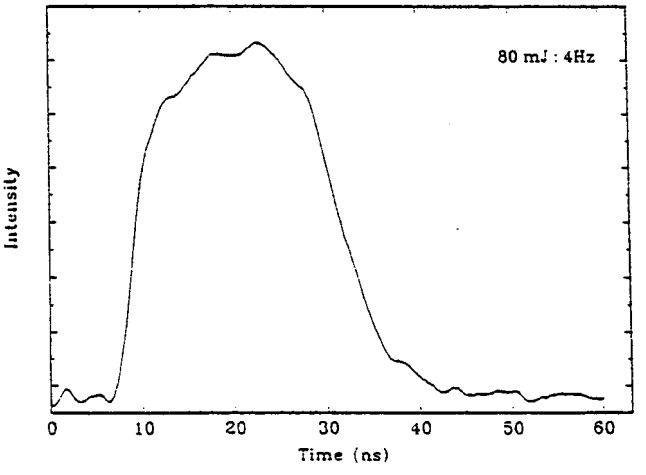

Fig. 9. Temporal profile of XeCl laser pulse at 308 nm (independent of repetition rate).

Laser Vaporization Thresholds

In the field of high power pulsed laser interaction with solids there has been a considerable discussion in the literature over the definition and interpretation of thermal evaporation vs. non-thermal "ablation" [14,15]. The distinctions center on whether the material removal is driven by thermal heating of the near-surface region or by direct bond-breaking. We have chosen to use the term "vaporization" to avoid introducing loaded issues. In a first set of measurements we have determined the pulse energy density at the threshold for vaporization. For our definition of vaporization threshold, we used the operational condition of surface damage visible easily in an optical microscope.

A summary of the threshold energy densities for ablation is presented in Table 1. Note that we are giving thresholds in terms of the incident pulse energy with no correction for the reflected fraction. Thresholds are affected by the specific heat and the heats of fusion and vaporization, but the optical absorption length and its dependence on wavelength is the most important factor in these thin-film materials. In all cases the threshold measurements were made with single pulses. In some cases the energy density was measured directly with a detector behind a 5 μm pinhole and heavy attenuation of the laser beam. In other cases, especially where all data had to be acquired within a few hours in a single visit to an applications lab, we inferred the energy density from an analysis of ablation spot sizes taken over a wide range of energy densities. Therefore the estimates of threshold energy densities should be treated with care since we estimate typical error limits at ±50%.

Wavelength-dependent effects are clearly seen in Table 1. In the strongly absorbing semiconductors CdTe and $CuInGaSe_2$ (CIGS), the ablation thresholds are low as expected, less than 0.5 J/cm^2 except for the case of CdTe at 1064 nm where the photon energy is below bandgap. The lowest thresholds for all materials are observed at 248 nm and 308 nm even though the excimer laser pulse duration is somewhat longer than the flashlamp-pumped YAG. These low thresholds arise from the very high absorption coefficients in the ultraviolet for all of these materials. Not surprisingly, the effects are particularly large for the conducting oxides (SnO_2 and ZnO) which are transparent at all the other wavelengths. Note that the ablation thresholds for SnO_2 and ZnO in the UV are about 1/10 of those observed in the green or infrared. Crystalline Si exhibits a much higher threshold for visible damage at 1064 nm which is right at the absorption edge.

It is interesting that little variation is observed in this damage threshold between the 250 ns Q-switched pulses and the mode-locked pulse trains at both 1064 and 532 nm. This is probably due to the fact that the mode-locked pulses are part of a train of about 25 pulses spaced by about 15 ns which is too little time for significant thermal diffusion. (See Discussion Section..) Thus the thin film gradually heats over a time scale of the duration of the full pulse train, 350-400 ns. Another contributing factor arises from the partial mode-locking which occurs in this laser even without active modelocking. (See Fig. 6b and Fig. 7b.)

For the transparent oxide materials there is little pulse-width dependence but they appear to be affected by non-linear absorption effects. ZnO in the visible and near infrared has the highest thresholds, but also has large spot-to-spot variations in the ablation thresholds presumably due to absorption processes which initiate at defects or interfaces. In addition we find that the ablation threshold is much lower if the ZnO has been irradiated by previous laser pulses even if these have not produced visible damage -- again presumably caused by laser-irradiation-induced defect centers.

At longer pulse durations, thermal diffusion during the pulse also becomes a factor. The effect of pulse duration is clearly evident at 532 nm where the 90 nsec pulse gives a threshold two to three times higher than the 8 nsec pulse, for most materials. Longer pulses allow for greater diffusion of heat into the film during the pulse, thus raising the threshold.

during the pulse, thus raising the threshold.
The threshold data appear somewhat anomalous for the cwp/ml-YAG laser which was operated with the modelocker on to give pulse durations of about 0.1 ns at either 1064 or 532 nm or with the modelocker off (but Q-switch still on) to give ~250 ns pulses at both wavelengths. The differences are small between the two pulse durations at either wavelength. However, this may be related to the fact that some modelocking occurred with this laser even with the active modelocker off. Furthermore the interpretation is complicated because the modelocked output consisted of the train of modelocked pulses rather than a single subnanosecond pulse. The thresholds for the green pulses, either modelocked or non-modelocked, appear to be unusually low. This might be related to the very low available pulse energy of the laser and the need to focus very tightly (although the focussed power density was measured with a 5 μm pinhole). The low thresholds in the green might also be an indication of some non-linear absorption effects occurring with the subnanosecond pulses. The threshold numbers for this laser system (0.1 ns & 250 ns @ 1064 nm; and 0.1 & 250 ns @ 532 nm) should be treated with caution.

Table 1: Threshold for Vaporization of Thin-Film Materials (J/cm²)

λ(nm), τ(ns)	E_{max} (mJ)	SnO_2	CdTe	Cu/Au	ZnO	CIGS	Moly	Si
1064nm, *0.1 ns*	1.1	1.8	0.8	0.9	5.8	0.14	0.87	5.8
1064nm, *250ns*	1.3	2.6	1.1	0.73	6.8	0.14	0.73	6.8
1064nm, *70ns*	2	4	1.5		7	0.5	1.5	
1064nm, *10ns*	500	2.4	0.65		3.9*	0.32	0.44	
532nm, *0.1 ns*	0.07	1.5	0.016	0.016	3.3	0.028	0.16	1.2
532nm, *250 ns*	0.014	1.6	0.017	0.021	>2.8	0.021	0.16	1.6
532nm, *90 ns*	2	5	0.22		12*	0.23	0.5	
532nm, *70ns*	1.5	6	0.07		10	0.07	0.7	
532nm, *10 ns*	200	4.5	0.10		3.5*	0.15	0.26	
511nm, *55ns*	2.0	3.4	0.10		0.6	0.1	1.0	
308nm, *15ns*	80	0.44	0.08		0.24	0.13	0.24	
248nm, *25ns*	400	0.22	<0.07		0.16	<0.08	0.32	

* highly variable

Optimum Energy Density for Scribing

One of the most important parameters associated with laser scribing is the speed of the cut. Clearly this is a function of the laser power, but also of the energy efficiency of the vaporization. Thus we have studied the vaporization depth as a function of pulse energy to identify the energy density needed to optimize the scribing rate. The relationship between increasing pulse energy density and the depth of material removed is given in Figs. 10 and 11. These data show the depth of material vaporized per pulse as measured by a stylus profilometer trace across the ablation spot. Each panel of Figs. 10 and 11 shows the laser wavelength and pulse duration. Recall that the data for the 0.1 ns pulse durations, at both 1064 and 532 nm, are for pulse trains of about 25 pulses and the energy density is that of the complete, Q-switched pulse train. Also, it should be noted that the data for 532 nm and 250 ns pulse duration were obtained with pulses which exhibited significant mode-locking. (See above.)

Fig. 12 shows similar results for single pulse vaporization depths obtained recently with the dlp-YAG laser at a) 1064 nm and b) 532 nm. Again, most of the thin-film PV materials were studied. The results are consistent with the other YAG laser data shown in Figs. 11 and 12.

Typical film thicknesses were about 2 μm except for SnO_2, which was 0.5 μm. Thus if the depth, shown in Figs. 10 & 11, completely saturates with increasing power, it is due to the limitation on film thickness.

For ZnO, except with the two excimer lasers, there was either no ablation or the entire film was blown away. Frequently the first pulse incident on a spot produced no visible effect, but the second pulse produced complete removal. The ZnO ablation was highly variable with high thresholds (values with * in Table 1) and very steep rises above threshold, giving indications that absorption for the non-uv wavelengths initiated at interfacial or bulk defect sites possibly enhanced by a first pulse.

Some general trends are evident. The uv pulses tend to reach their maximum ablation rates at the lowest energy densities of any of the lasers. This is consistent with the lower thresholds observed in Table 1. However, the vaporization depth per pulse also tends to saturate at rather low values. The lower energy thresholds are related to the higher photon energy which sees typically a higher film absorption coefficient. The saturation in vaporization depth is undoubtedly related to higher energy loss in the plume vapor.

Another general trend is that the longer pulse durations can produce deeper craters with a single pulse. In many cases, the full film thickness can be vaporized with a single pulse. However, the pulse energy required is large. (It should be noted that the horizontal axes in Figs. 10 and 11 are logarithmic.) For example, the full ~2 μm thickness of CdTe, CIS, or Mo can be vaporized with a single pulse at λ=1064 nm, τ=250 ns with the energy density of about 3 J/cm^2. By contrast, a single pulse at λ=248 nm, τ=25 ns with energy density of 0.5 J/cm^2 will vaporize roughly 0.1 μm of these materials. Thus six pulses at 248 nm with a total energy of 3 J/cm^2 will remove about 0.6 μm, noticeably less than the single, 3 J/cm^2, 250 ns pulse at 1064 nm. However, efficiency of material removal is not the sole criterion in choosing a laser scribing engine. Other factors such as beam quality, beam delivery, available energy per pulse, and repetition rate are very important. Some of these are addressed below.

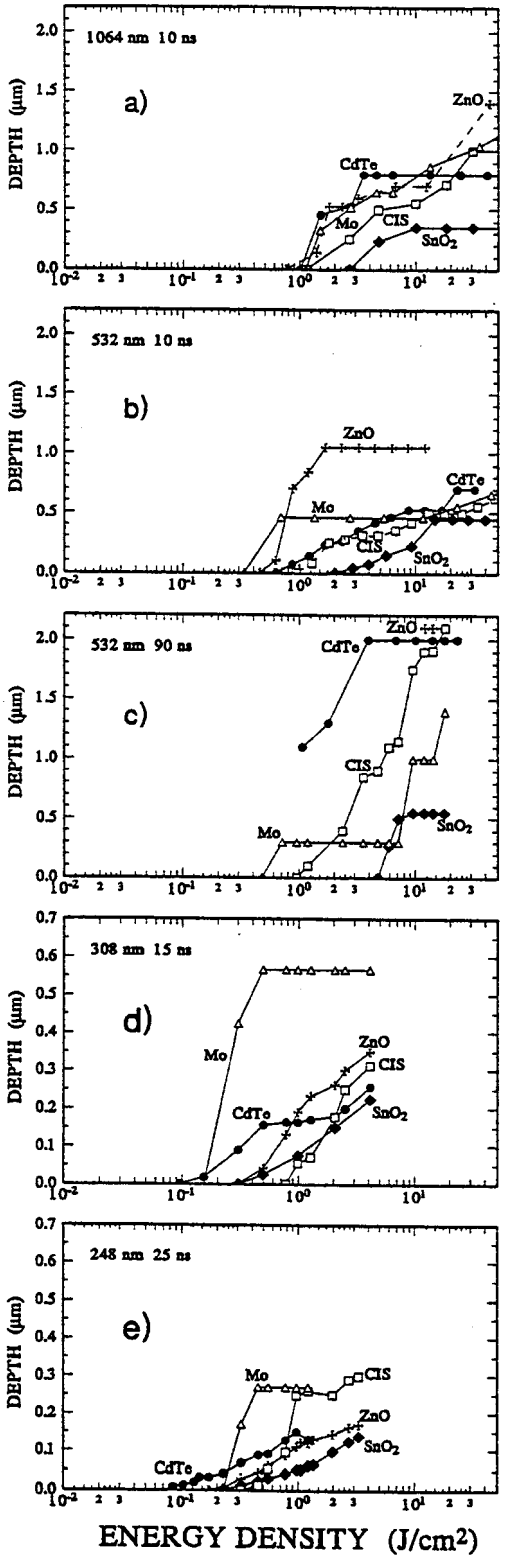

Fig. 10. Thickness removed per pulse vs. energy density for five thin-film materials and five different types of laser pulses. Note the change in vertical scale for d) and e).

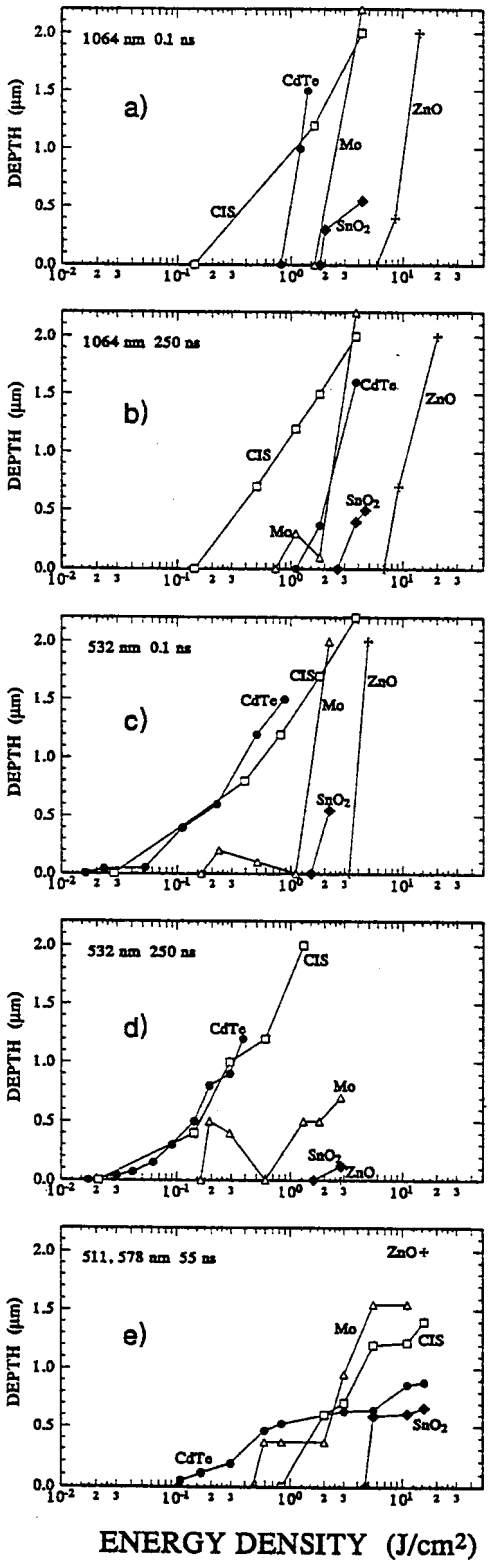

Fig. 11. Thickness removed per pulse vs. energy density for five thin-film materials and five more types of laser pulses.

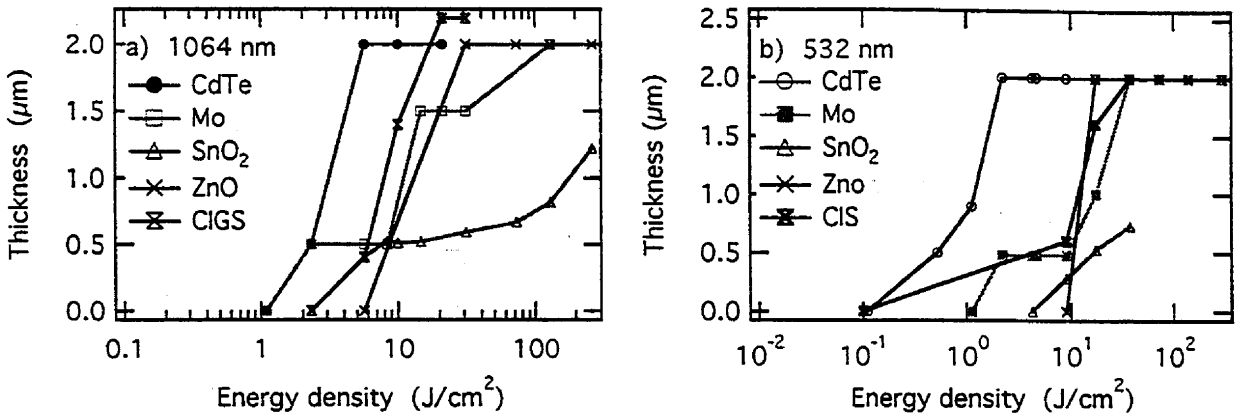

Fig. 12. Thickness removed per pulse vs. energy density for diode-laser-pumped YAG at a) 1064 nm and b) 532 nm and several different thin film materials.

Beam delivery to the film

Beam focusing was done with a spherical lens for the quasi-cw Nd:YAG lasers and for the copper laser. For the 10ns flashlamp-pumped Nd:YAG and the excimer lasers, cylindrical focussing was also used. We have found that cylindrical focusing can have distinct advantages, particularly by allowing one to reach an optimum energy density with a very narrow line width. In general we found it to be helpful to work with an energy density near that which gives the optimum vaporization rate since this leaves a smaller heat-affected zone surrounding the scribe and makes it easier to control the scribe depth.

From the data of Figs. 10 and 11, we can infer conditions which will facilitate optimum utilization of the laser pulse energy. Thus for the Cu-vapor laser operating with 16 W of power at 8 kHz PRF, the energy per pulse was 2 mJ. With a beam divergence of 0.1 milliradian, a 12.5 cm focal length lens will focus the beam to a 25 μm diameter spot and if we conservatively estimate that 1/3 of the energy should fall in the central region of intensity above the ablation threshold, the energy density in this region will be ~100 J/cm^2. From Fig. 11e we may estimate that the optimum efficiency for CdTe occurs at about 0.5 J/cm^2 at which point each pulse removes about 0.5 μm. (CIGS would require somewhat higher pulse energies.) Six pulses should remove a 3 μm layer. This laser either could be split into ~20 beams with a scan speed of ~20 cm/sec, or focused to a line image with dimensions of 0.5 cm by 25 μm. At 8 kHz PRF, the scan speed should then be ~4000 cm/sec along the long axis of the focal spot. This is a situation clearly calling for multiple beam delivery to the workpiece!

Similar considerations for the other lasers yield the following: (1) For 2 W of power from the cwp-YAG at 1 kHz, cylindrical focussing to produce a 25 μm x 500 μm spot should work well for CdTe, CIGS, and Mo (See Fig. 10c.) with translation at 25 cm/sec. (2) For our flp-YAG at its maximum PRF of 30 Hz, and its pulse energy of 100 mJ, the optimum focus would have to be ~25 μm x 15 cm. Finally, (3) with the XeCl excimer laser at a PRF = 100 Hz, 100 mJ/pulse, and ideal focussing to a 25 μm x 15 cm line, the translation speed would need to be 150 cm/s, or multiple beam splitting should be used.

For the KrF laser, we used a beam homogenizer and optical delivery system which projected a demagnified slit image onto the film plane. This produced very clean scribes. It is worth noting that this type of laser could have sufficient pulse energy (500 mJ) to image across a full panel width (~40 cm) so that no lateral beam scanning would be necessary. In this case it should be possible to vary the pulse energy or focussing as the beam penetrates the film to avoid damage to an underlying film or substrate, or to defocus the beam to remove any "burrs" or ridges at the scribe edges. See discussion of scribe profiles below.

Cylindrical Focussing

Too much energy density at the center of the focal spot can result in undesirable effects. We have seen, for example with the flashlamp-pumped YAG at 1064 nm on CdTe films, that one can get a complete scribe but there is a large heat-affected zone surrounding the scribe. When spherical lens focussing (f=10 cm) is used, the energy density at the center of the scribe line was 50 times the ablation threshold so that the weak fringes of the focal spot have enough energy density to damage a wide swath around the scribe. See Fig. 13a. By contrast, the use of a 6 cm cylindrical focussing lens allows one to reduce the energy density at the center of the scribe. Figure 13b shows results obtained with cylindrical focussing with about 60% of the energy density used for Fig. 13a. Furthermore, the long line image allows higher scan speed. In this case the scan speed with the cylindrical lens was about 18 times greater than for the spherical lens.

The transverse discharge of the XeCl excimer laser leads to a rectangular beam profile with high angular divergence in the horizontal dimension. Therefore, for some of our work we obtained uniform irradiation

of an aperture close to the laser output and imaged the aperture onto the film with a 10 cm spherical lens. When cylindrical focusing was used, we irradiated a rectangular aperture and imaged this with two cylindrical lenses. A 50 cm cylindrical lens controlled the long dimension of the image on the film and a 6 cm cylindrical lens focused the short dimension onto the film. Typical film-to-lens distances were 40 cm and 6 cm respectively. For scribing, the film was translated parallel to the long axis of the image. To facilitate alignment of the lens axis with the scribe direction, the 6 cm cylindrical lens was mounted in a rotatable holder.

We have found that cylindrical focusing is advantageous for several reasons. For most of the lasers in this study, the available energy density is much higher than the optimum values wich can be inferred from Figs. 10 and 11. Focusing with two cylindrical lenses allows one to adjust the focused spot to attain the optimum energy density for most efficient vaporization. For example the excimer lasers reach optimum energy densities at relatively low values which can be achieved with a long, narrow focus geometry. Secondly, the line image allows for several overlapping pulses which then minimizes the effects of any laser power fluctuation or dust in the beam path. Third, the line image can be shaped to provide higher power at the leading edge and lower power at the trailing edge, if, for example, one wants to limit the scribe depth to terminate at the interface with the underlying film layer.

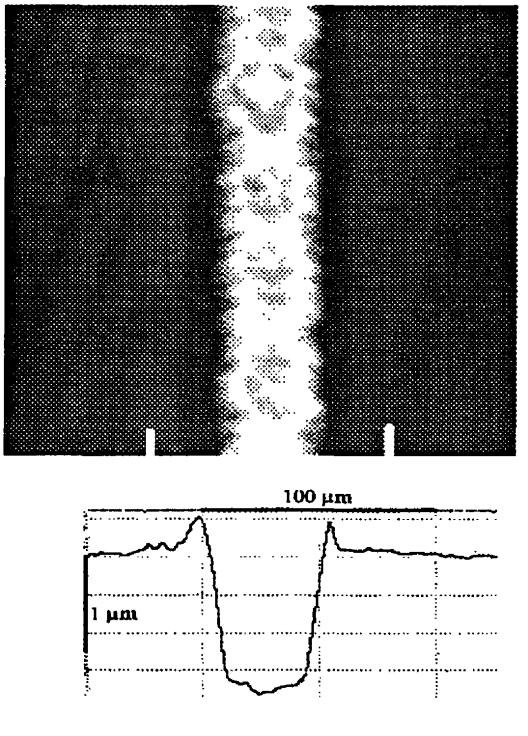

Fig. 13a. Optical micrograph and stylus profilometer trace of flp YAG scribe in CdTe with 5 J/cm^2 at 1064 nm, 10 Hz, 0.09 mm/s, and 10 cm spherical lens focussing.

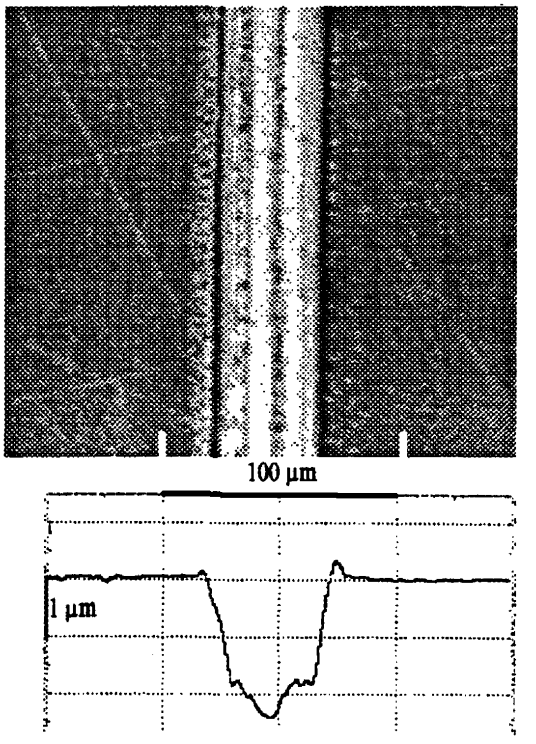

Fig. 13b. Optical micrograph and stylus profilometer trace of flp YAG scribe in CdTe with 3 J/cm^2 at 1064 nm, 10 Hz, 1.6 mm/s, and 6 cm cylindrical lens focussing.

Scribe Morphology

The section on Optimum Energy Density for Scribing provided data which can be used to obtain the highest vaporization rate (fastest scribing) for all of the lasers and materials combinations we have tested. However, for laser scribing to be successful in thin-film PV applications, it is also necessary to know further details about the scribe such as the scribe morphology and the composition at the scribe bottom or sides. In this section we discuss the morphology. It is known that for some combinations of materials and lasers the morphology of the scribe is poor. For example, for films of Mo and ZnO on glass, we have observed, for some lasers, cracking of the film and film delamination along the scribe edges. In other situations, there can be a substantial heat-affected zone along the sides of the scribe. In the following discussion we provide some typical examples of scribe morphology. Scribe profiles were studied with an optical microscope and with a stylus profilometer.

Semiconductor Films

Both of the semiconductor films studied have high absorption for all of the laser wavelengths except for CdTe at the YAG fundamental (1064 nm). The binary semiconductor, CdTe, seems to be the easier semiconductor to scribe with good morphology. For example, even at 1064nm where CdTe is nominally transparent, CdTe can be scribed reasonably well. Especially with CIGS, however, considerable effort may be necessary to maintain clean scribe profiles and to avoid positive ridges at the edges of the scribe. These ridges appear to arise from melt phase at the scribe edges. Surface tension and momentum recoil from the vaporization plume lead to formation of these ridges at the edges of the scribes. We have seen similar but less severe effects with CdTe for some conditions. Details and examples are provided below.

Figs. 14 and 15 show optical micrographs and stylus profilometer traces of scribe lines obtained with the cwp-YAG laser at relatively high pulse energy density (~7.5 J/cm^2) on CIGS and CdTe. This energy density is about 30 times the threshold energy density for damaging the surface. (Note that the threshold was obtained for 90 ns pulses at 1 kHz whereas these scribe lines were obtained for 180 ns pulses at 5 kHz.) Comparison of the scribes shows strong similarity for the two materials. For both semiconductors one observes evidence of a melt zone surrounding the scribe with ridges protruding significantly above the plane of the film. This is clearly undesirable. A very high scan speed was chosen in order to try to separate the adjacent laser spots. The optical micrograph shows that the scan speed was too slow by about a factor of two to separate the individual spots and the deepest craters occur along the line of maximum overlap. The profilometer shows that the full 2 μm film thickness was vaporized at the overlap. A slightly slower speed should give a cleanly separated scribe. However, improved scribe morphology probably would require somewhat lower power density and greater pulse overlap.

A similar study was done with the Cu-vapor laser. In this case the wavelengths are similar to that of the frequency doubled Nd:YAG above. Typical results for CdTe are shown in Fig. 16. At a power density of 16 J/cm^2 (approximately 80 times the damage threshold) a scribe speed of 9 cm/s or about 5-6 overlapping pulses, (Fig. 16a) the scribe has reached full depth. However, the edges of the scribe have noticeable ridges. At much lower power density (0.5 J/cm^2) and correspondingly lower scribe speed (1.35 mm/s), the scribe shows no evidence of ridges (Fig. 16b). For Fig. 16b, the 10 cm lens was defocused by about 2 mm. Although the scribe width here was about 140 μm, there is no evidence of protruding ridges around the scribe line. In this case the peak energy density was only 0.5 J/cm^2 or about twice the vaporization threshold but with about 40 overlapping pulses.

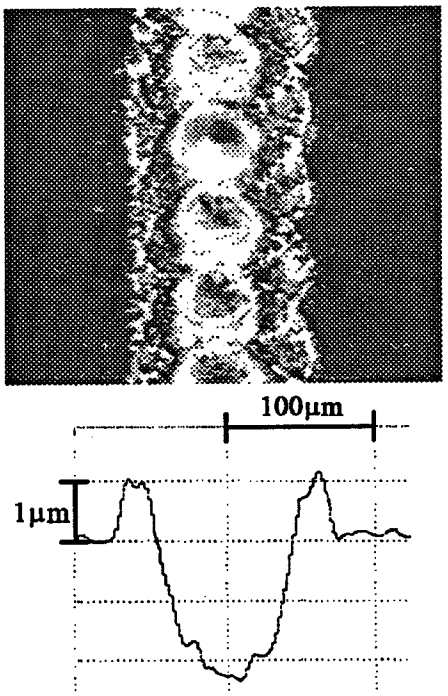

Fig. 14. Optical micrograph and stylus profilometer trace of cwp YAG (532 nm) scribe in CIGS at 7.5 J/cm^2, 5 kHz, and 25 cm/s.

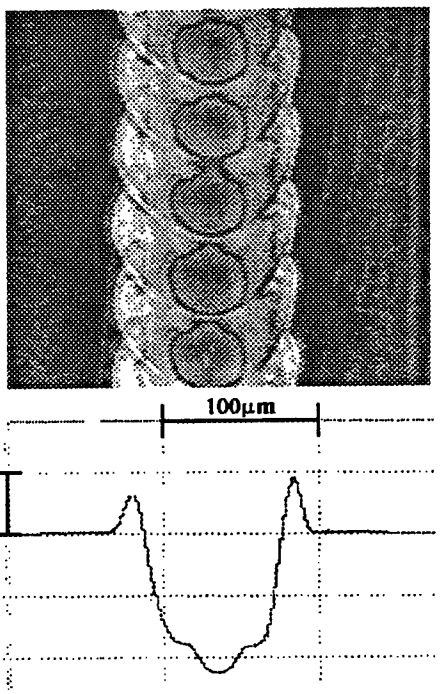

Fig. 15. Optical micrograph and stylus profilometer trace of cwp YAG (532 nm) scribe in CdTe at 7.5 J/cm^2, 5 kHz, and 25 cm/s.

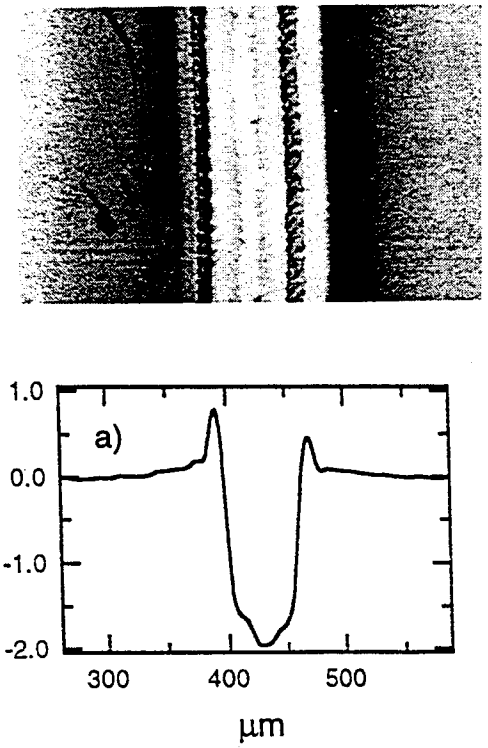

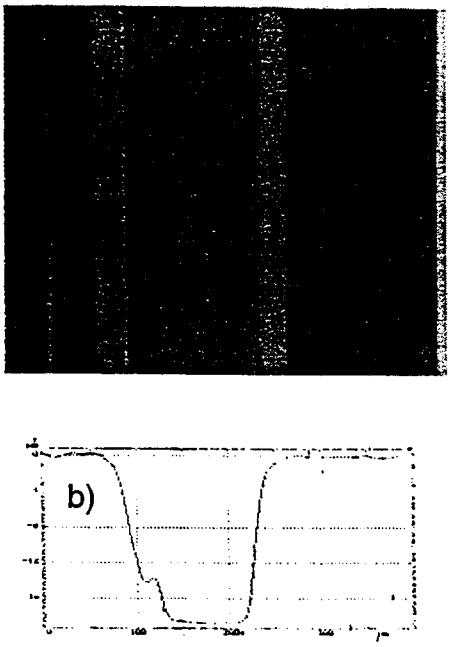

Fig. 16. Optical micrographs and stylus profilometer traces of 8 kHz Cu-vapor laser scribes in CdTe with a) 16 J/cm^2 @ 90 mm/s, and b) 0.5 J/cm^2 @ 13.5 mm/s.

These examples illustrate that in general the use of power densities far above the threshold for damage, can be used to give very deep vaporization depths with a single pulse but it may also lead to positive ridges along the scribe as the melt is pulled to the side by surface tension and pushed by the recoil momentum of the vaporization plume. The results also illustrate, however, that careful choice of power density can produce a scribe morphology which is quite satisfactory. The data also indicate that tighter focus conditions lead to increased tendency to form ridges along the edges of the scribe. This is plausible since the gradients in temperature, surface tension, and recoil momentum are smaller for the broader focus conditions. These would suppress the formation of the positive ridges.

For copper-laser scribing of CIGS (Fig. 17) a narrow scribe line was achieved with a tight focus and an energy density of ~2 J/cm^2. Here the pulse duration is about 1/3 that of the CWP YAG so that the peak power density is similar. Again positive ridges are observed along the edges of the scribe which extend about 1 μm above the plane of the film.

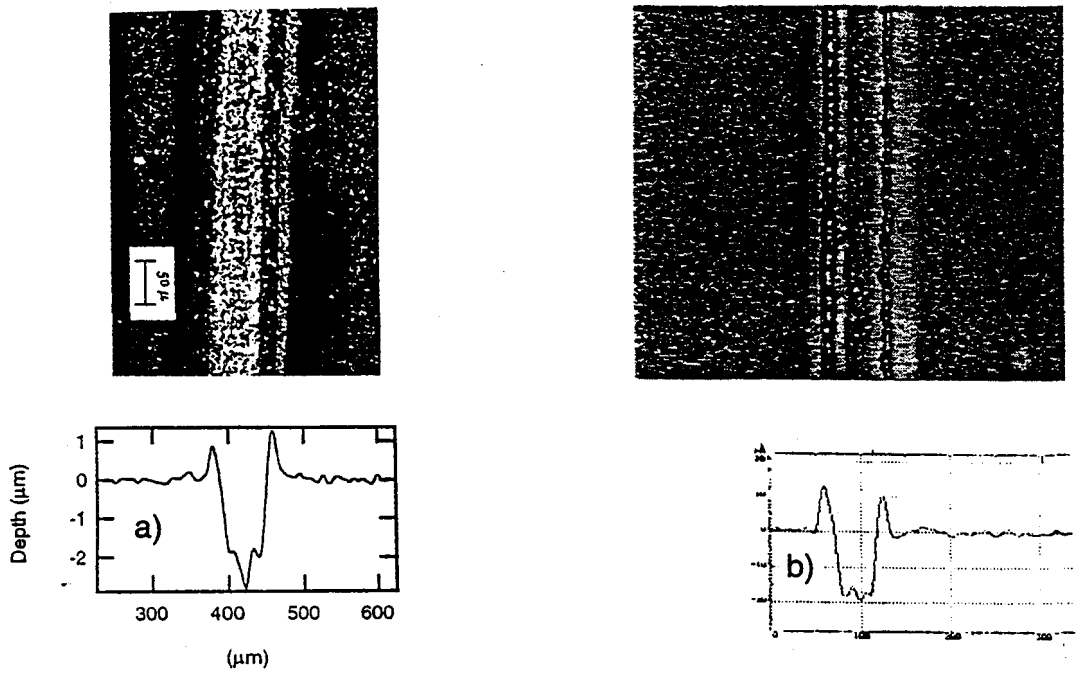

Fig. 17. Optical micrographs and stylus profilometer traces of 8 kHz Cu-vapor laser scribes in CIGS with a) 16 J/cm^2 @ 90 mm/s and b) 2 J/cm^2 @ 13.5 mm/s.

Both excimer lasers produced excellent scribe morphology for CdTe. For the XeCl excimer in our laboratory, we used a cylindrical focus and scanning along the cylinder axis. For the Kr F excimer, used at the applications lab of Lambda Physik, we took advantage of a beam homogenization and imaging system to produce long and narrow scribe lines without scanning. Figs. 18 and 19 illustrate the results. Fig. 18 shows a typical scribe profile for the XeCl laser scanned at 1 mm/s at a power density of 3.5J/cm^2 (~40 times the damage threshold). Fig. 19 shows the profilometer trace across scribe lines obtained with the KrF laser at low pulse energy density (0.23 J/cm^2 or about four times the damage threshold). Note that at this energy density the profile is quite square and the scribe is self-limiting at the CdTe/SnO_2:F interface. The conditions of Fig. 19 with the sharply defined image projected onto the film and consequent high intensity gradient at the edge of the scribe, significant ridges are produced. We believe that the gradients contribute to the ridges projecting up to 0.75 μm above the ~2 μm thick film. The ridges do decrease with more applied pulses. Also, we suggest that it may be advantageous to use a softer focus to minimize these positive ridges. However, we have not had an opportunity to explore variations of focus with the KrF excimer laser.

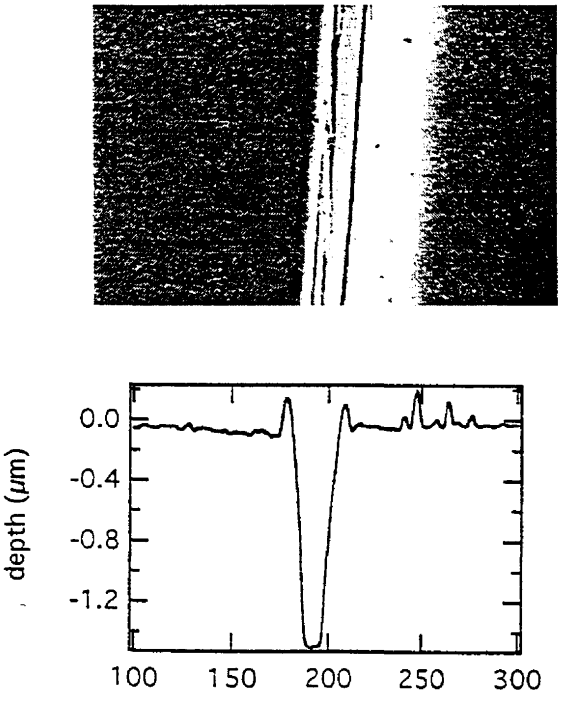

Fig. 18. Optical micrograph and stylus profilometer traces of XeCl excimer scribe line in CdTe (cylindrical focus, 3.5 J/cm^2, ~15 pulses, scanned).

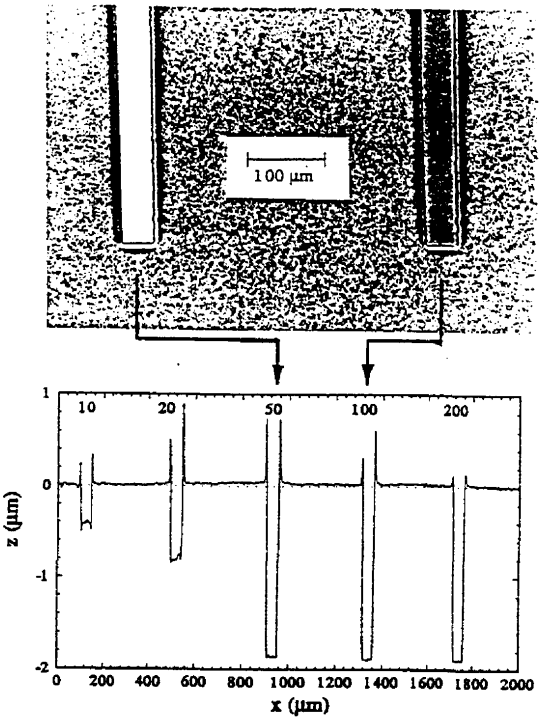

Fig. 19. Optical micrograph of the end of two KrF excimer scribes and profilometer trace across five scribes in CdTe on SnO_2 for 10, 20, 50, 100, and 200 pulses at 0.23 J/cm^2.

For the quaternary semiconductor, CuInGaSe, the scribe morphology is poorer in every case. Laser scribing should be able to provide acceptable scribes, however. Figures 20 and 21 provide examples of the scribe profile for the two excimer lasers in CIGS. Part of the difference in scribe morphology relative to CdTe results from the greater roughness of the starting film. However, Fig. 21 gives evidence of considerable residue from a melt phase during the scribing. In this case the 248 nm laser power (unscanned) was about ten times the threshold for surface damage. Roughness of the as-deposited surface is observable on the wings of the profilometer trace. With five pulses at this ~1 J/cm^2, there is considerable islanding in the bottom of the scribe with significant probability for bridging of the scribe. If

these islands are conducting, as we believe they may be, there would be shunting and likely a significant increase in interconnect series resistance.

Although for CdTe, the vaporization (damage) threshold is much lower than for the underlying SnO_2 film--leading to the possibility of a self limiting scribe as shown in Fig. 19, such is not the case for the excimer lasers in CIGS on Mo. (Figs. 10d and 10e indicate that the Mo threshold is a little lower than the CIGS.) Reviewing the data of Figs. 10 and 11, suggests that the best wavelength/pulse duration combination for CIGS/Mo to achieve a self limiting scribe is the 1064 nm / 250 ns pulse from the cwp/ml-YAG laser running without the mode-locker. In other words, the longest pulse duration possible with the infrared wavelength. This result is at least partially consistent with the observations of Ref. 7 which reported some success with a continuous YAG laser at 1064 nm.

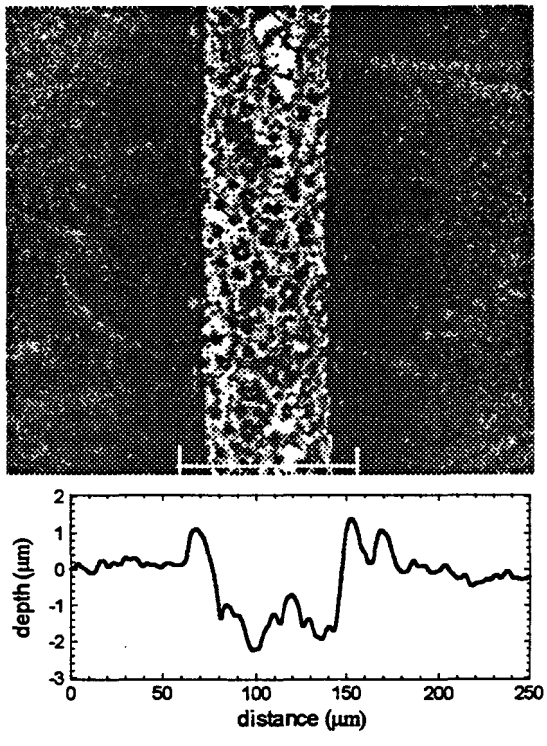

Fig. 20. Optical micrograph and stylus profilometer traces of XeCl excimer scribe line in CIGS (2 J/cm², ~10 overlapping pulses).

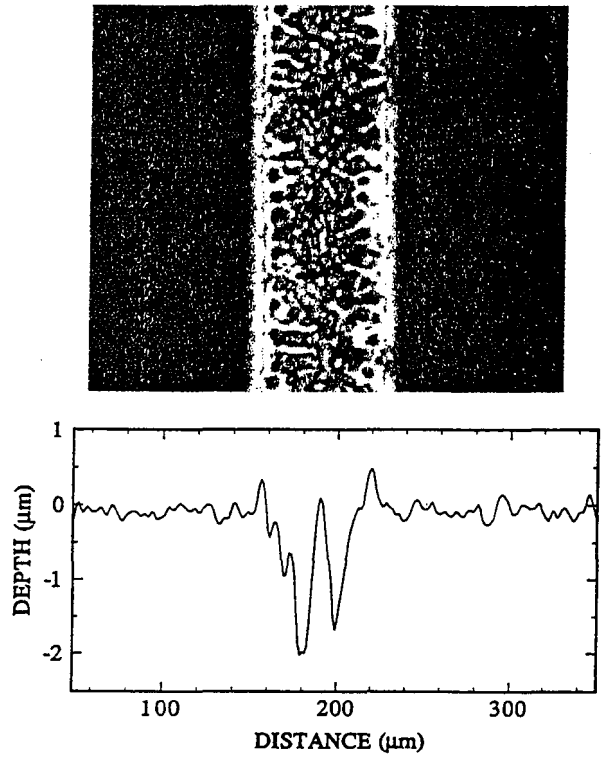

Fig. 21. Optical micrograph and stylus profilometer traces of KrF excimer scribe lines in 2.2 μm CIGS for 5 pulses at 0.96 J/cm².

The problem of ridges

Problems of ridge formation were pronounced with the use of the 250 ns pulse length YAG laser. We believe that these problems were aggravated with the long pulse duration and therefore long melt time and also from the need to achieve a very tight focus with this low energy-per-pulse laser to scan the range of pulse energies needed for Fig. 11. Figures 22 and 23 show both the vaporization depth and ridge height as a function of pulse energy density for single shots on rf sputtered CdTe and CIGS, respectively. Similar effects are seen in CdTe and CIGS in which the ridges are consistently 1/4 to 1/3 of the depth of the vaporization spot. Note that these data are taken from profilometer traces of single-pulse vaporization spots. These figures show very clearly that for CIGS, the data for the infrared pulses and the green pulses are quite similar but for CdTe the threshold for the ir pulses is much higher and the amplitudes of both scribes and ridges are very strong functions of pulse energy density--not surprising since the room temperature absorption at 1064 nm in CdTe is very weak and non-linear absorption sets in at high power.

The data of Figs 22 and 23 were obtained with relatively low energy pulses, tightly focussed from the cwp/ml-YAG. Note that, for this configuration (wavelength, pulse duration and focus) it apparently would not help particularly to use lower pulse energies (and more pulses to penetrate the full film thickness) since the ridge height is roughly a constant fraction of the scribe depth. However, we have found that the formation of these ridges is dependent on the focal spot size of the laser. This was first observed in work with the Cu-vapor laser where we found that results with a soft focus produced no ridges (Fig. 16c) whereas work with a tight focus produced significant ridges (Figs. 16a&b). In the latest work with the dlp-YAG we tested the effect of the focus. Fig. 23 provides a series of profilometer traces across scribes obtained with the frequency-doubled beam. The focal distance of the 10 cm spherical lens was adjusted from best focus (10 cm) to 13.8 cm and then to 15.7 cm. The laser pulse energy was simultaneously increased to keep the energy density approximately constant (as is evidenced by the scribe depth). Note that for the soft focus, there are no ridges present, whereas with the tightest focus, the ridges are about 1/3 the scribe depth. The data for the tightest focus is consistent with the data shown in Fig. 22 which utilized a very small spot size (~25 μm). These results indicate that the problem of ridge formation along the scribe can be controlled. We suggest that another approach might be to use, in conjunction with cylindrical foucssing, a soft focus on the trailing edge of the line image.

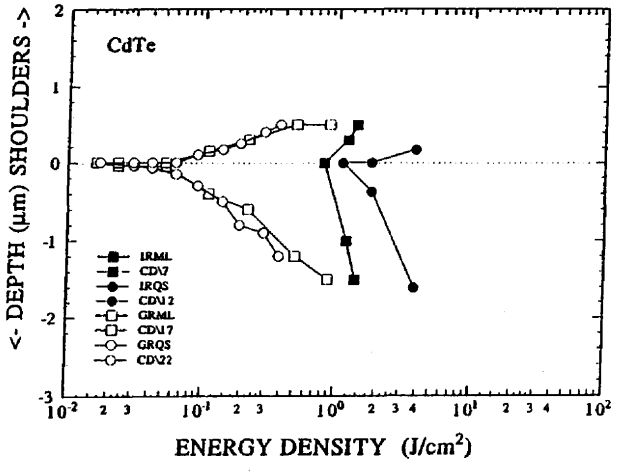

Fig. 22a. Analysis of ablation spots in CdTe comparing the height of ridges with the depth of the scribe. ■, ● 1064 nm; □, ○ 532 nm.

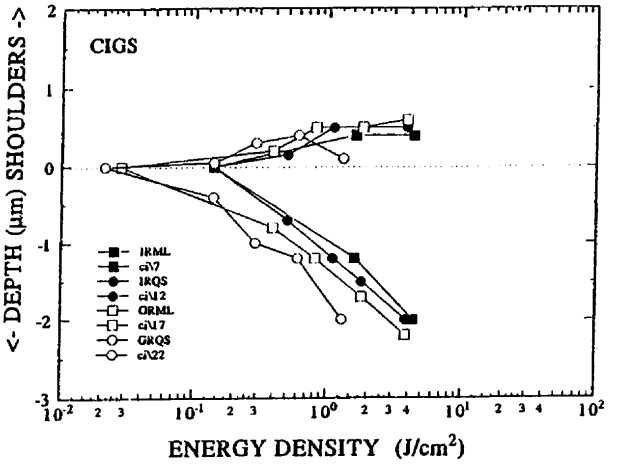

Fig. 22b. Analysis of ablation spots in CIGS comparing the height of ridges with the depth of the scribe. ■, ● 1064 nm; □, ○ 532 nm.

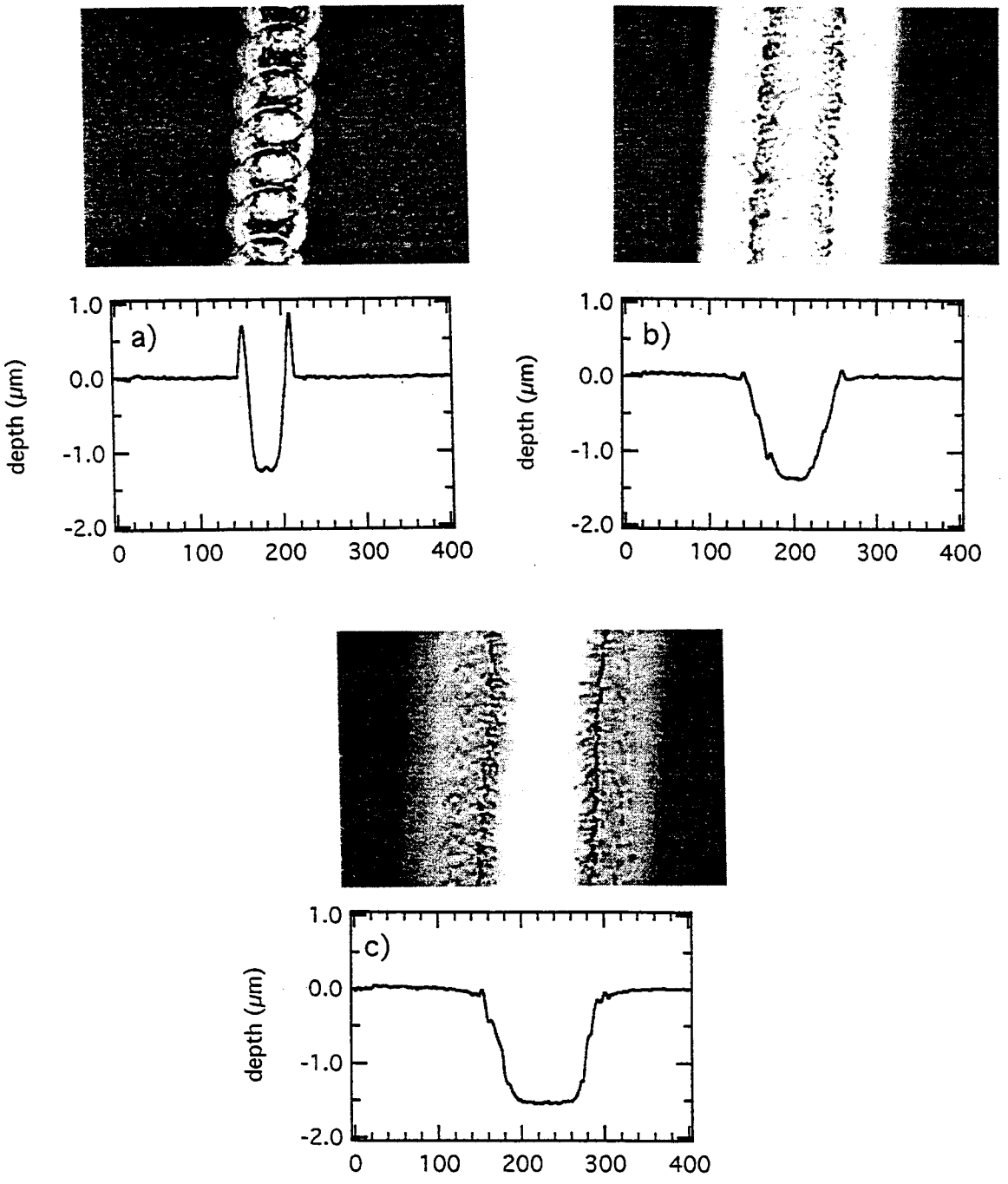

Fig. 23. Optical micrographs and profilometer traces of dlp-YAG scribes at 532 nm for different positions of the 10 cm focussing lens. a) 10 cm, 9 J/cm^2, b) 13.8 cm, c) 15.7 cm. For b) and c) the beam energy was increased by factors of four and eight, respectively to keep the power density approximately constant

Transparent Conducting Oxides

The two TCO materials considered in the study had quite different scribing characteristics. The SnO_2:F was relatively easy to scribe cleanly at all wavelengths even though the threshold was high in the visible and near-infrared, as expected from the low absorption coefficient. The scribe profile obtained with the Cu-vapor laser is shown in Fig. 24. The very steep side walls are probably a consequence of the non-linear absorption for the green and yellow wavelengths of this laser in the essentially-transparent TCO. Apparently there is enough residual absorption, possibly due to free carriers, to initiate the vaporization process with little chipping or cracking of the film at the edges of the scribe.

The situation is quite different for ZnO:Al. (See Fig. 25.) In this case the visible and near-infrared pulses provide very unreliable scribing. It appears that a single pulse on a virgin spot of the film will not initiate vaporization except at very high power densities. However a second or subsequent pulse often will have a relatively low threshold for vaporization. Once absorption does start, almost always the entire film is blown away. The morphology suggests that absorption may initiate at the ZnO/glass interface creating a high pressure vapor bubble which then lifts off the film, often with substantial tearing of the surrounding film. For ZnO:Al the adhesion is lower than for SnO_2 and the film tends to flake off as shown in Fig. 25, for pulses from the copper-vapor laser. For a scribe obtained with the flp Nd:YAG, Fig. 26 shows that it does not help to use a shorter pulse duration of 8 nsec vs. the 55 ns for the Cu-vapor laser. There is slight marking of the underlying glass confirming that the onset of absorption may be occuring at the ZnO/glass interface.

By contrast, when the XeCl excimer laser is used for ZnO, the scribe boundaries are very smooth with no evidence of flaking. See Fig. 27. This is consistent with the fact that the absorption is very strong at the 308 nm wavelength of the excimer. For 248 nm scribing with the KrF (Fig. 28) and an unscanned beam, the scribe profiles were also very clean. The data of Fig. 29 on the transmission through the SnO_2:F and ZnO show that there is strong absorption for both the 308 and 248 nm beams. Thus, we conclude that for scribing of SnO_2 as the first layer on glass, almost any laser wavelength and pulse duration will work satisfactorily, in spite of the fact that the material is quite transparent. However, ZnO appears to require uv wavelengths to obtain reliable scribing. Certainly, we have found that the two excimer lasers work well for a single layer of ZnO on glass. Further discussion is provided below for the case of ZnO as a top contact layer on CIGS structures.

Although we have not addressed issues of scribing of SnO_2 or of InSnO (ITO) when it is deposited on top of another thin film (e.g., the case of an ITO top contact on a-Si:H cells), we may anticipate that a laser with uv wavelength will be advantageous. This would point to the use of an excimer or possibly a frequency tripled or quadrupled YAG, although the tripled, 355 nm wavelength may not be strongly enough absorbed in the case of ITO.

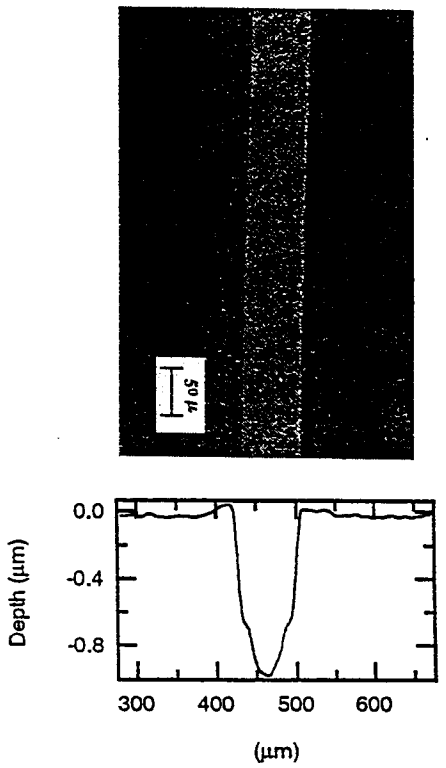

Fig. 24. Optical micrograph and stylus profilometer trace for Cu-vapor scribe line in SnO_2 @ 100 J/cm^2, 180 mm/s.

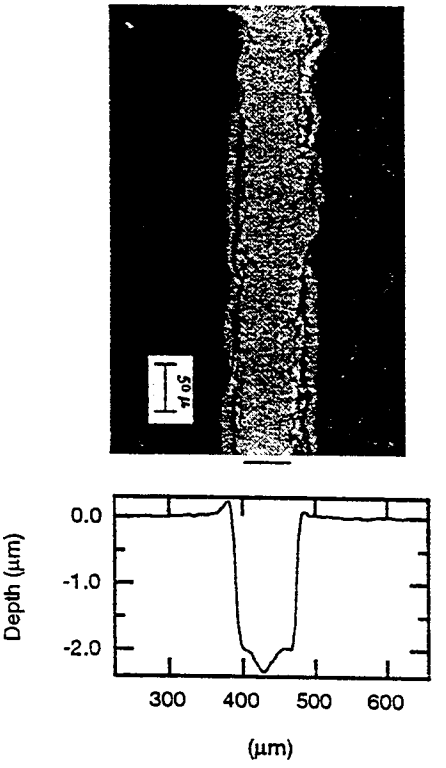

Fig. 25. Optical micrograph and stylus profilometer trace for Cu-vapor scribe line in ZnO @ 100 J/cm^2, 180 mm/s.

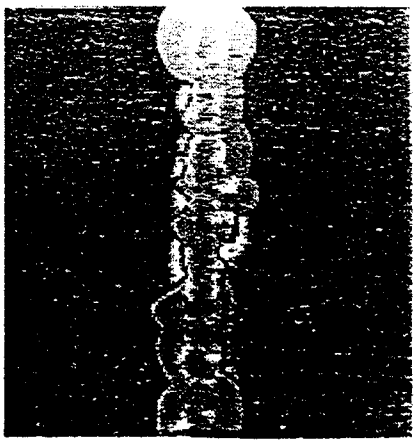

Fig. 26. Optical micrograph of flp-YAG(8 ns) scribe line in ZnO @ 15 J/cm^2, 10 Hz, 1mm/s.

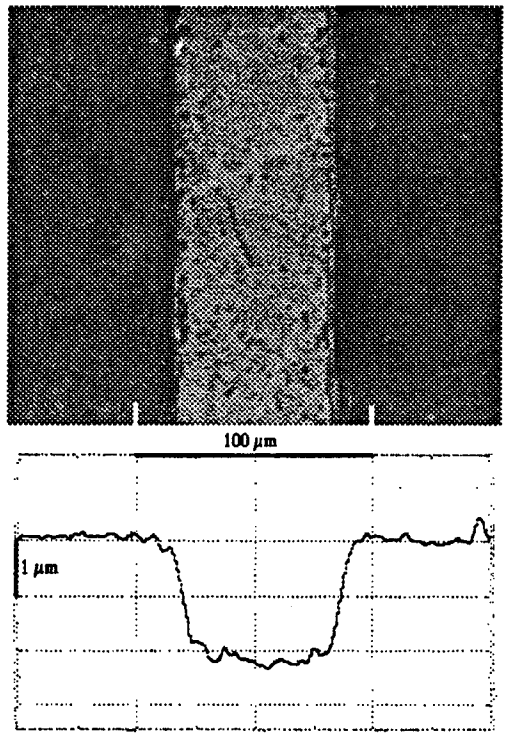

Fig. 27. Optical micrograph and stylus profilometer trace for XeCl excimer scribe line in ZnO @ 2.5 J/cm^2, 20 Hz, 1 mm/s.

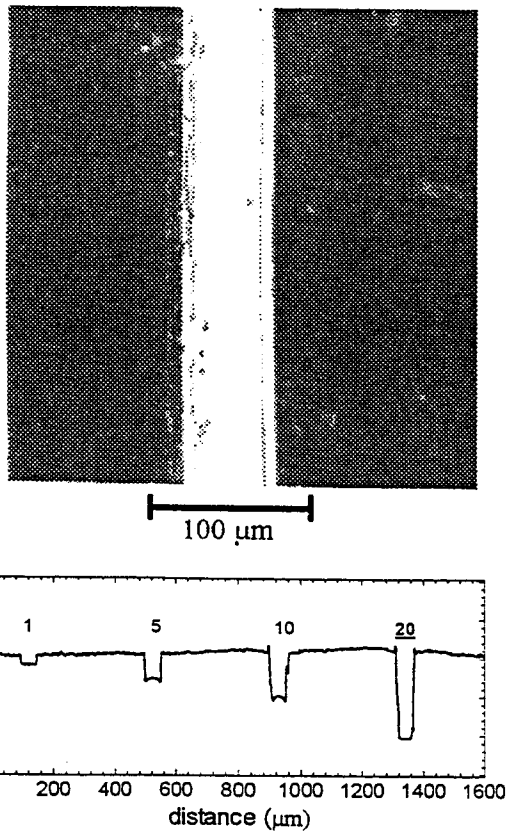

Fig. 28. Stylus profilometer trace across KrF scribes in ZnO for 1, 5, 10, 20 pulses @ for 1.22 J/cm^2. Optical micrograph is for 20 pulses.

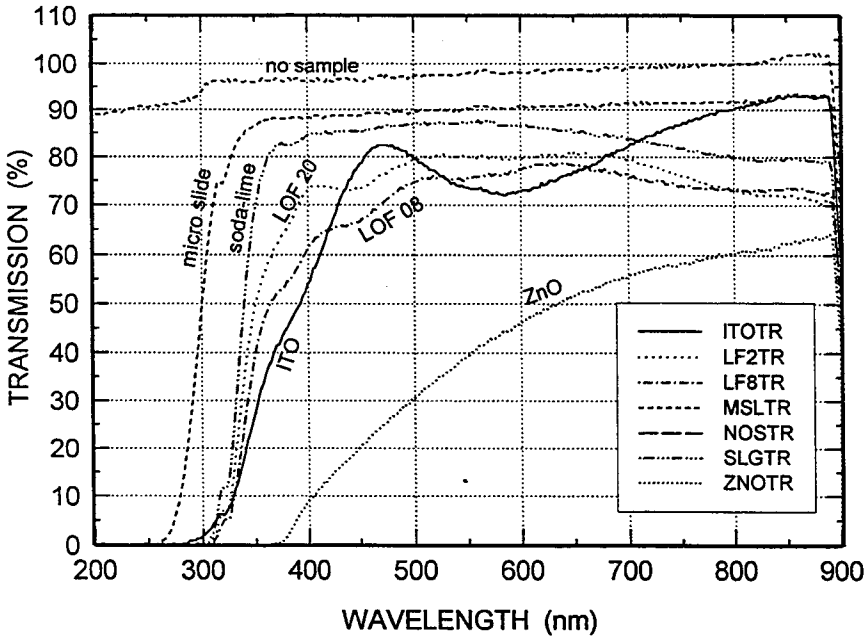

Fig. 29. Double-beam optical transmission of SnO_2:F (LOF8 and LOF20), 0.28µm sputtered ITO, 2µm ZnO, 1mm and 3mm soda-lime glass substrates.

Metals

Metals are very strongly absorbing (and reflecting) at all wavelengths near the visible so one would not expect any serious wavelength-dependent effects in laser scribing. In fact, we have found difficulties in scribing of Mo only with the copper laser under some conditions. We have also done some tests of scribing of gold contacting layers on CdTe with some of the lasers.

Fig. 30a shows a "scribe" of a Mo film with the Cu-vapor laser. Clearly there was too much average heat load on the film which produced cracking and delamination. However, in a second study with this laser, we found that a tighter focus, and higher scanning speeds could produce acceptable scribes of Mo on glass. This scribe is shown in Fig. 30b. Comparison of the two scribes illustrates that the choice of focus condition and translation speed are important in obtaining a high quality scribe.

With the XeCl laser, a clean scribe is readily obtained for the same Moly film. This is shown in Fig. 31. The scribe morphology appears similar to that in ZnO as shown in Fig. 26 above. The similarity is presumably due to the fact that optical absorption is very high at 308 nm in both materials and the short pulse duration minimizes heat flow during the pulse.

Scribing of Mo with fundamental and frequency-doubled YAG lasers is also quite possible. One interesting feature of Mo vaporization appears in the spot profile of Fig. 32. In this case there was no scanning of the film which received, in this area, only a single pulse. The 1.4 μm thick film vaporized in three distinct layers. These layers correspond to the fact that the Mo was deposited with some periodic rotation of the substrate in front of the sputtering gun. This film probably made four passes over the source. In this profile no separation appears between the second and third layer. Possibly there was some slight oxidation at the two interfaces within the Mo film which gave rise to "quantized" vaporization.

Figures 33 and 34 below illustrate the scribe profiles which may be obtained with 70 ns pulses at 1064 nm and with 70 ns pulses at 532 nm, respectively.

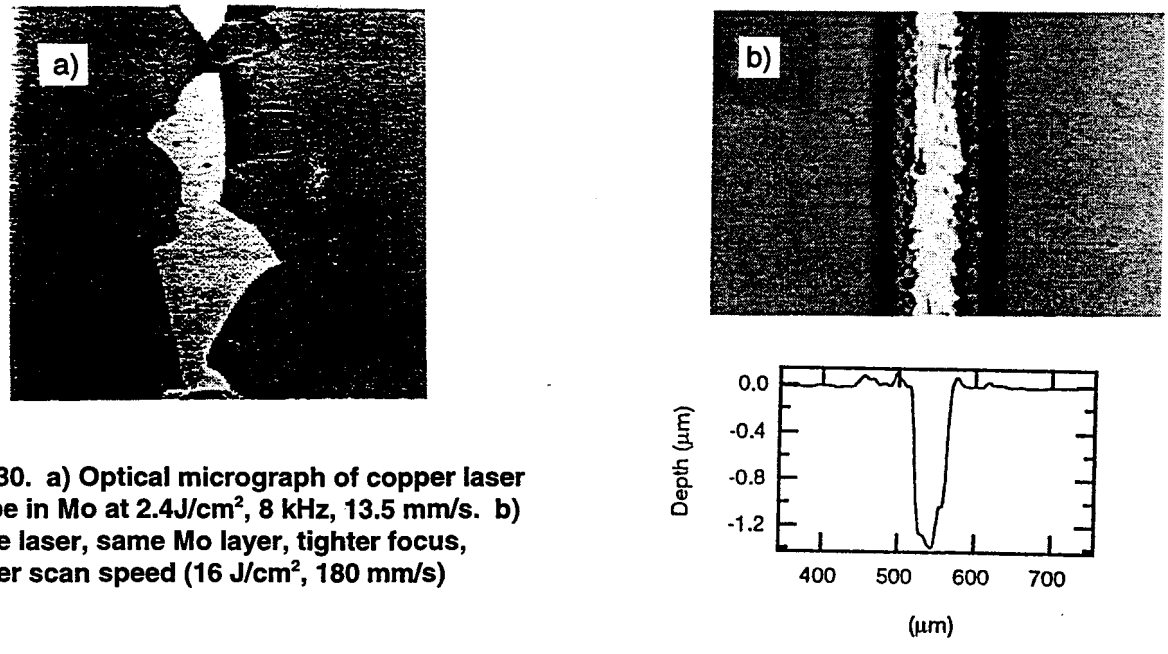

Fig. 30. a) Optical micrograph of copper laser scribe in Mo at 2.4J/cm², 8 kHz, 13.5 mm/s. b) Same laser, same Mo layer, tighter focus, higher scan speed (16 J/cm², 180 mm/s)

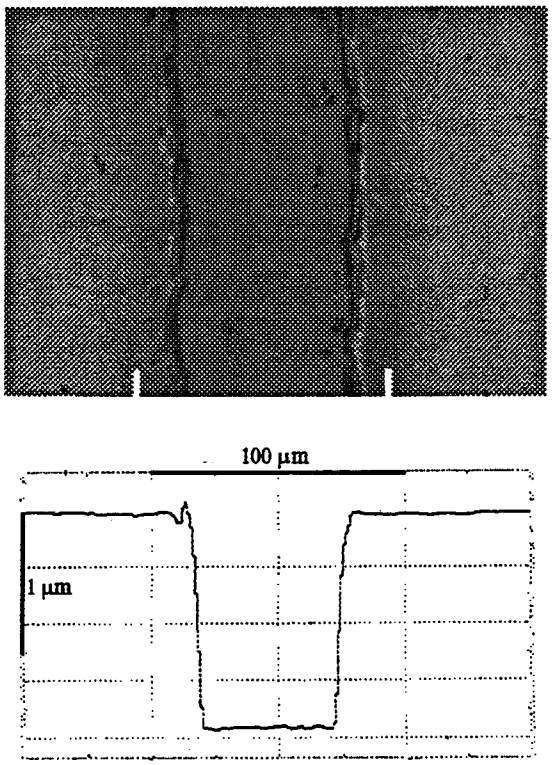

Fig. 31. Optical micrograph and profilometer trace of XeCl scribe in Mo (1J/cm², ~10 pulses).

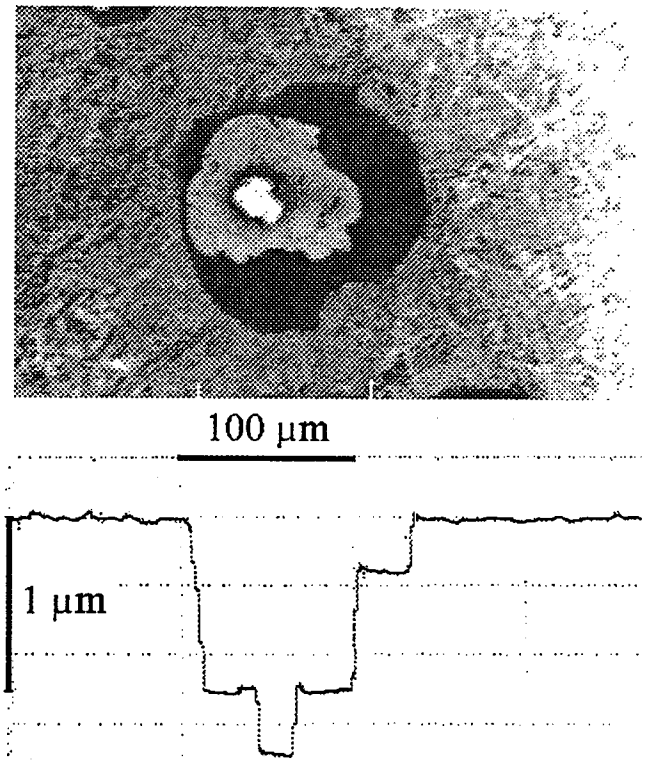

Fig. 32. Micrograph and profile of a single shot @532nm, 18 J/cm², 8 ns.

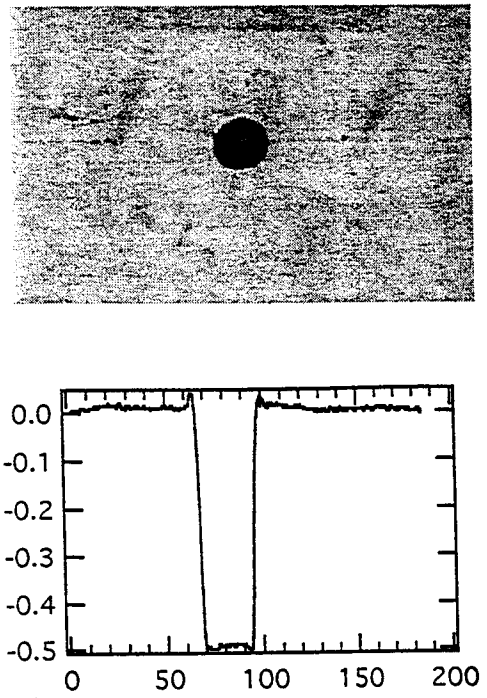

Fig. 33. Micrograph and profile of ablation spot in Mo obtained with single pulse of 70 ns dlp-YAG @ 1064 nm, 10 J/cm²

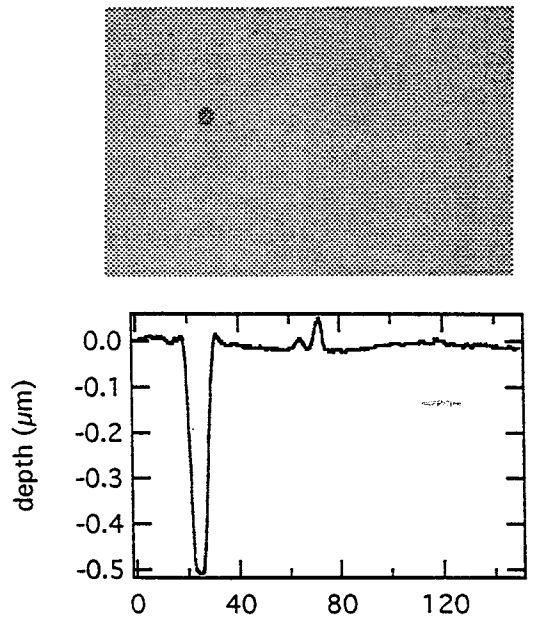

Fig. 34. Micrograph and profile of ablation spot in Mo obtained with single pulse of 70 ns dlp-YAG @ 532 nm, 1.1 J/cm²

Glass-side scribing

Back-side or glass-side scribing is possible for two of the thin-film PV systems studied, Mo/glass and CdTe/SnO_2/glass. In these cases, the energy efficiency can be much higher, especially for thicker films, with very little evidence of a heat-affected zone observable from the surface. Glass-side scribing may be an important option, and necessary, for thicker films. We have found that scribing of CdTe films of 10 to 20 μm from the film side is difficult because of the surface roughness due to faceting. We expect that this might also be a problem for films which have a porous surface structure such as obtained with screen printing or spray pyrolysis. These problems arise from the fact that laser scribing tends to remove a relatively uniform thickness for each pulse and if the surface roughness is a micron or more, it may be difficult to terminate the scribe at the TCO or glass interface. Furthermore, if high power densities are used to obtain high vaporization rates in film-side scribing, there is likely to be significant damage surrounding the scribe--in a wide heat-affected zone.

Glass-side scribing of thick CdTe films appears to have real advantages. Of course this cannot be done with a uv laser due to absorption in the glass. A comparison of the morphology of film-side vs. glass-side, 532 nm flp-YAG-laser scribes in 2 μm thick CdTe is shown in Fig. 35. Fig. 35a shows the scribe obtained with the beam incident from the film side and Fig. 35b shows the result for the beam incident on the glass side. We find that it is possible, with appropriate power density (~ 1.5 J/cm^2) to obtain full removal of the CdTe and have little damage to the SnO_2 film underneath.

A comparison of film-side and glass-side scribing of Mo is shown in Fig. 36. Parts a) and b) show the results obtained with spherical lens focusing of the cwp/ml-YAG. The profile of the film-side scribe shows evidence of debris ejected during scribing. We expect that this may be eliminated with appropriate gas flow across the film during scribing. The glass-side scribe shows ridges which may be due to some

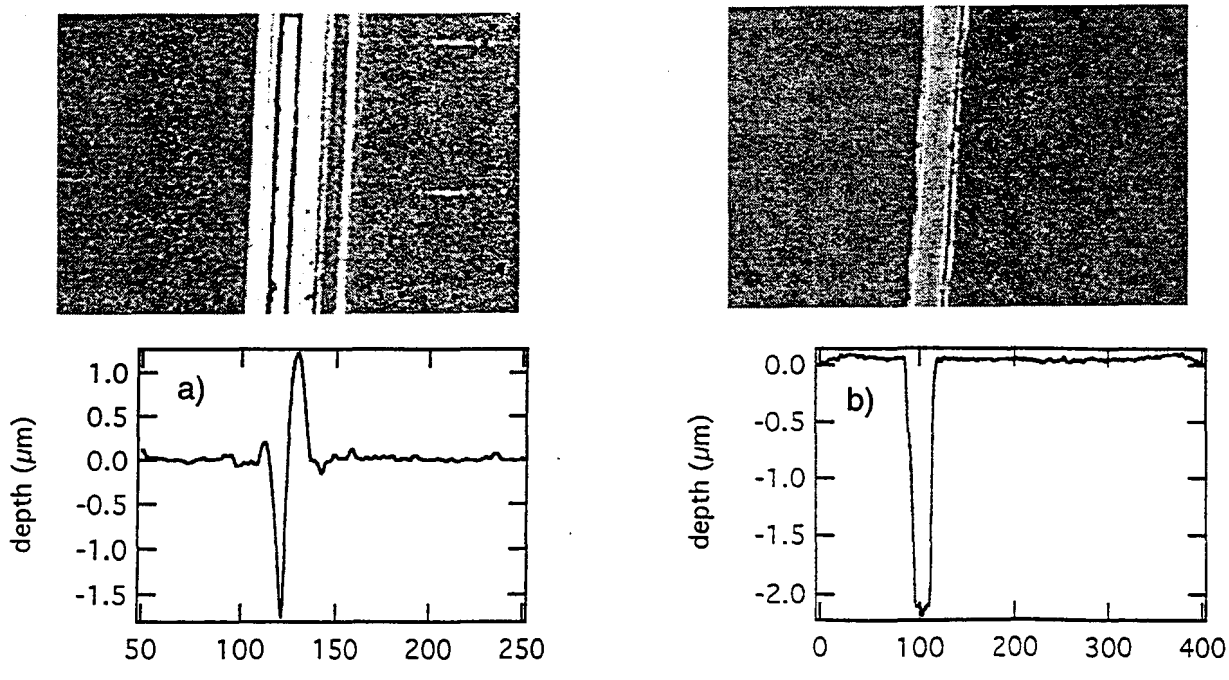

Fig. 35. Flp-YAG laser (532 nm) scribing of CdTe in the structure: glass/SnO_2/CdS/CdTe comparing: a) film-side scribing at 1.5J/cm^2, 1 mm/s, and b) glass-side at 1.5J/cm^2, 1 mm/s. (both cyl. focus)

curling ofthe edges of the film. The profilometer trace is limited by the tip resolution in both of these traces since the beam focus was very tight for this laser. Fig. 36c shows the results for backside scribing using the flp-YAG. Here the scribe was wider as a result of using a cylindrical lens and a laser with higher beam divergence. It should be noted that our glass side scribing of Mo has so far yielded poorer results in interconnected submodule tests, but it not yet clearly identified as related to the side of incidence.

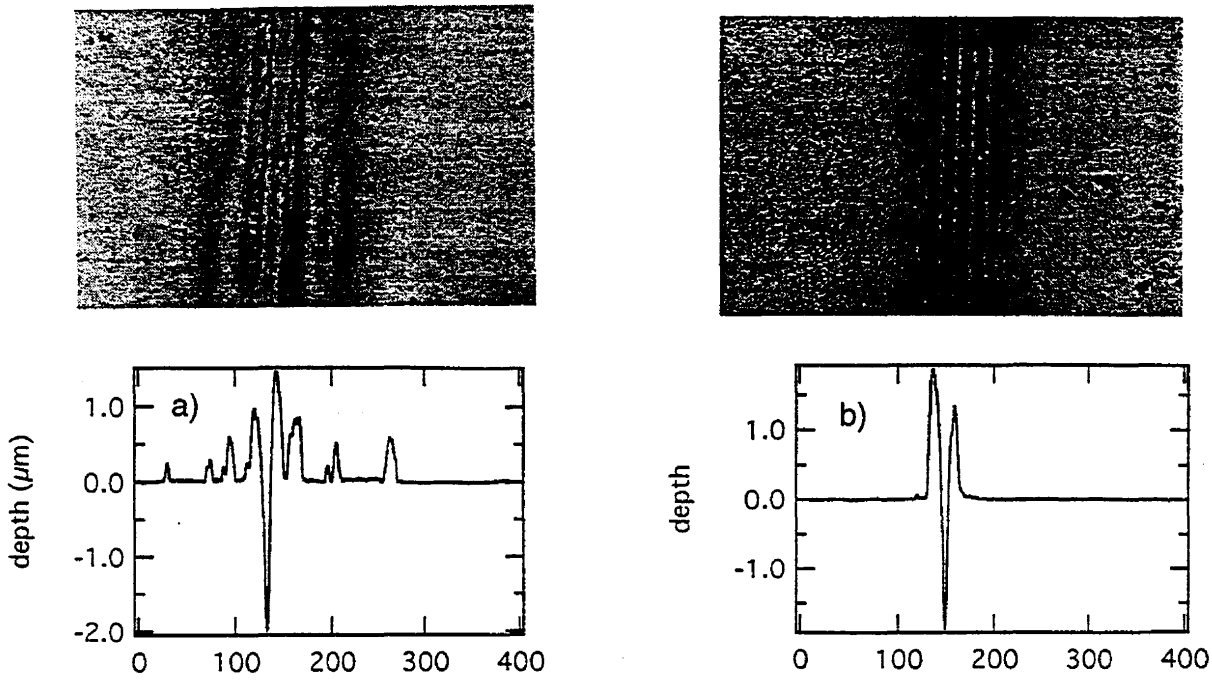

Fig. 36. A comparison of scribing of Mo on glass obtained with a low power spherical-lens-focussed cwp/ml-YAG: a) film side, b) glass side, and c) a cylindrical-lens-focussed flp-YAG incident on glass side and less tightly focussed.

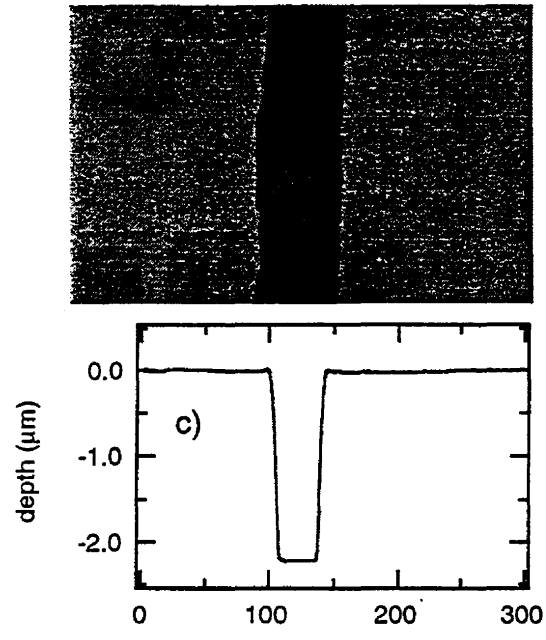

Interconnected submodules

The most challenging task for laser scribing, other than cutting rough films of 15 μm from the film side perhaps, is to achieve an isolation scribe through a metal layer on CdTe or a ZnO layer on CIGS. In order to test for possible problems which might not show up in profilometry traces or optical microscopy, we fabricated some small integrated submodules in both CIGS and sputtered CdTe materials. The CdTe structures were fabricated entirely at UT. In the case of the CIGS the fabrication procedure involved three depositions at ISET and three laser scribes at UT with a final return to ISET for testing--that is, a total of six long-distance exchanges. Therefore the scribe separation was kept fairly large. Results must be regarded as tentative, especially for the CIGS, because of the long-distance exchange of samples.

The typical interconnect schemes for CIGS and CdTe modules are shown in Figs. 37. For CIGS, the typical layer thicknesses are: Mo (1-2 μm), CIGS (2 μm), CdS (30 nm), ZnO (1-2 μm). The ZnO may be a double layer consisting of a thin undoped and a thicker doped layer. The typical CdTe module consists of the glass superstrate, SnO_2:F (0.5 μm), CdS (30 nm), CdTe (4 μm), metal. (Actually the best cell performance, to our knowledge has been achieved with relatively thick doped graphite contacts (50 μm thick or more) and others use ZnTe (2 μm) before the metal.)

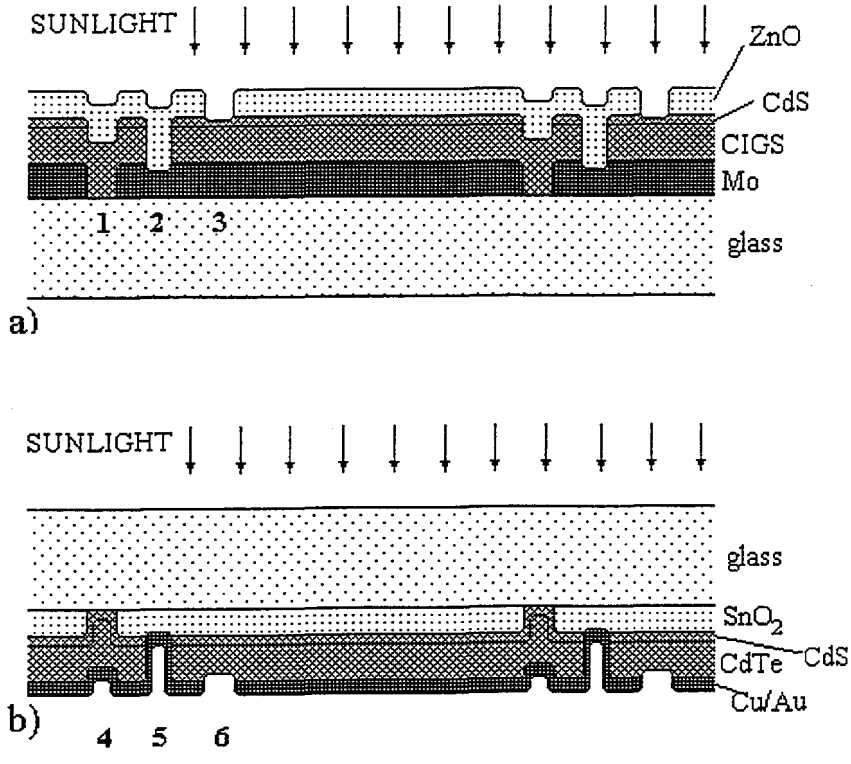

Fig. 37. Typical interconnect scheme a) for CIGS-based modules, and. b) for CdTe-based modules. Note that the glass thickness and interconnect separation are not to scale. Typical scribe widths are 40 μm, scribe separations are 100 μm, interconnect separation is 5-10 mm, and the glass thickness is ~ 3-5 mm.

Initial results on CIGS structures were encouraging, although somewhat inconsistent, probably related to the necessity for repeated cross-country exchange of samples. In order to test more directly for interconnect resistance, special structures were designed and fabricated to obtain current flow mainly through the low resistance Mo layer. (See lower sketch in Fig. 38.) Two schemes were used for the CdTe structures as shown in both top and bottom sketches of Fig. 38. The lower structure was designed to allow the current to flow mainly through the top Au metallization which has much lower sheet resistance than the SnO_2:F. Tests of interconnect resistance in CdTe showed somewhat lower resistance for CdTe scribed through the glass. Further evaluations of these structures and the reproducibility of contact and shunt resistances are still in progress.

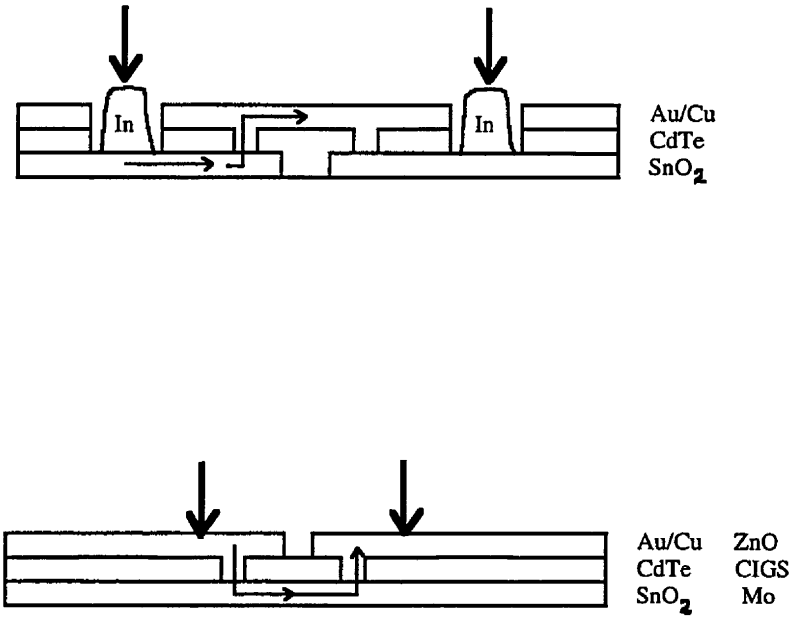

Fig. 38. Structures designed to test for series resistance of interconnects CdTe modules (upper) and both CdTe and CIGS modules (lower).

Discussion

In this section we provide some discussion of the most important parameters involved in determining the energy density thresholds (for various wavelengths and pulse durations) and in understanding the factors which can be used to reduce the formation of ridge structures along the sides of scribe lines in the two semiconductor materials. The important materials parameters are the optical absorption length and the thermal diffusivity with some contribution possibly from the surface tension.

Thermal diffusion length

Consideration of thermal diffusion and optical absorption lengths in various materials will suggest how these ranges of pulse durations are important. Thermal diffusivity, D, is related to the thermal conductivity, κ(J/cm-s), the specific heat capacity, C_p (J/g-K), and the density, ρ(g/cm^3), by the following:

$$D = \kappa/\rho C_p \ [cm^2/s].$$

The thermal diffusion length is then

$$\ell = (Dt)^{1/2} \ [cm].$$

For example, in the case of CdTe at room temperature, κ=0.058 W/K-cm, $C_p \cong 0.205$ J/g-K, ρ=5.86 g/cm^3, so that D = 0.049 cm^2/sec.

Thus, during a 10 ns pulse the thermal diffusion distance is $\ell \sim 0.22 \times 10^{-4}$ cm = 0.22 μm. Similarly, during a 100 ps (0.1 ns) pulse ℓ = 0.022 μm and for a 300 ns pulse, the diffusion distance during the pulse is ℓ = 1.2 μm. Thus, for the longer Q-switched Nd:YAG pulses (~90ns or ~300 ns) the laser-deposited thermal energy will diffuse substantially (0.66 μm or 1.2 μm) into a 2-3 μm thin film of CdTe. Room temperature diffusion coefficients for our thin film materials are given in Table 2. T_B and T_M are the boiling and melting points respectively.

Table 2:Thermal Properties of PV-Related Thin Films*

	SnO_2	CdTe	Cu	Au	ZnO	CIS	Mo	Si
T_B (K)			2835	3129			4912	2953
T_M (K)	1903	1365	1358	1337	2248	1600	2896	1685
ρ(g cm^{-3})	6.85	5.86	8.96	19.3	5.68	5.77	10.2	2.33
C_p (J g^{-1} K^{-1})	0.34**	0.20	0.38	0.129	0.49	0.30	0.25	0.70
κ (W cm^{-1} K^{-1})	0.30**	0.058	4.0	3.2	0.23	0.037	1.38	1.24
D (cm^2 s^{-1})	0.13	0.049	1.16	1.27	0.084	0.022	0.54	0.76

* Ref. 16 ** Ref. 17

Optical absorption length

For most of the thin film materials of interest for photovoltaics, the linear absorption coefficient is reasonably well known at the wavelengths of the lasers used in this work. In the cases of the transparent conducting oxides, the linear absorption is shown in Fig. 29; however, it is possible that non-linear absorption is important at the higher pulse energies. In this case, the effective absorption length is much more difficult to estimate. These data of Fig. 29 were measured on a double beam spectrometer (Varian model DMS 300). For films with considerable roughness, such as LOF SnO_2 and especially the ZnO, the

energy absorbed is better measured with an integrating sphere. However, the present data will provide an upper limit to the absorption.

For example, the 532 nm pulse incident on CdTe is absorbed in a very shallow surface layer ($d = 1/\alpha = 0.13\mu m$.) Therefore, for a single 100 ps pulse, the thermal energy will diffuse a negligible distance ($\ell = 0.022\ \mu m$) compared with the absorption length. Thus, the energy will be absorbed in a thickness determined entirely by the absorption length.

Nonlinear absorption effects also will be much different for the different laser pulse durations. A 250 ns pulse of energy 1 J/cm^2 will have a peak intensity (irradiance) of about 4 MW/cm^2 whereas the same duration pulse made up of a train of twenty-five 100 ps mode-locked spikes separated by 10 ns each will have a peak intensity of 400 MW/cm^2! Any process which is sensitive to peak intensity such as two-photon or three-photon absorption will be very much stronger when exposed to the train of mode-locked pulses. If the onset of surface damage were determined by the peak intensity at the surface (or the electric field amplitude) then the damage threshold for the modelocked pulse should be lower by a factor of 100. If, on the other hand, the onset of visible surface damage were determined by the point at which the absorbed energy is sufficient to bring the surface temperature somewhat above the melting point, then a single, 100 ps pulse should require an energy lower by roughly the ratio of the two thicknesses, $0.022\ \mu m / 0.13\mu m = 0.17$. Unfortunately, this cwp/ml-YAG laser does not provide a *single* picosecond pulse but a train of about 25 with amplitudes which vary smoothly through the Q-switched pulse. A comparison of the data of Fig. 11c and 11d, and well as the low thresholds shown in Table 1 provide some evidence of non-linear effects. Most of our observations, however, are best explained by a thermal diffusion/melting point model and linear absorption.

The formation of ridges along the sides of scribe lines can be explained by material flow during the melt phase which persists for some time after every pulse of the laser. This material flow can be understood from considerations of momentum recoil from the ablation plume which exerts a downward force which is largest at the center of the laser spot and decreases toward the edges. Ridge formation should also be assisted by surface tension effects and the dependence of surface tension on temperature. Surface tension decreases as temperature rises toward the boiling point. As a consequence the surface tension will be higher at the edges of the spot than at the center. The result of these two mechanisms is to pull the hot, liquified semiconductor toward the edges of the spot with the consequence that, following a scribing pass, there will be ridges surrounding the scribe line. However, these driving mechanisms imply that one may be able to control and greatly reduce the amplitude of the ridge formations by reducing the energy gradients along the laser pulse. Thus if a wider spot is used, the ridges should be reduced. Also it should be possible to shape the profile the focussed spot to reduce the ridges. Thus, for example, if the spot has significant coma with the tail trailing the high intensity head, one should expect a reduction of the ridge formation.

We have tested the effect of defocussing the laser pulse to produce a wider spot and the effects are consistent with this model. Figure 23 showed traces of scribes in CIGS made with the diode-pumped Nd:YAG system for three different focus conditions. Our interpretation is that the softer focus condition reduces the pressure gradient (recoil momentum gradient) and also reduces the surface curvature which thereby reduce the driving forces for ridge formation.

Conclusions

We have determined the threshold power densities for the onset of ablation from thin films of CdTe, $CuInSe_2$, SnO_2:F, ZnO:Al, gold, and molybdenum for 12 different wavelength/pulse duration laser systems. Optimum energy density for most efficient removal of material during scribing is strongly dependent on the wavelength of the laser and to a smaller extent on the pulse duration. The optimum energy densities range from 0.5 J/cm^2 for the 532 nm, 8 nsec YAG pulse on CdTe to 0.2 J/cm^2 for the excimer laser at 308 nm on CIS. Poor scribing performance was seen with the 1064 nm beam on CdTe and all lasers except excimers on ZnO. Excellent scribe profiles were observed with the excimer lasers on all materials including ZnO.

The two uv (excimer) lasers have relatively low optimum efficiencies or material removal rates (~0.2 μm per J/cm^2) as opposed to the longer duration (70 to 250 ns) pulses of the cwp-YAG and dlp-YAG lasers which give efficiencies of up to ~3 μm per J/cm^2.

We have found significant advantages to the use of cylindrical lens focussing for the higher pulse energy laser systems with the suggested possibility that the excimer lasers could be delivered, in principle, to a line image which covers the entire module width.

Threshold pulse energy data for the various thin films explain the observed ease of obtaining clean scribes in CdTe with self-limiting depths at the CdTe/SnO_2 interface. In the case of CIGS/Mo the threshold data suggest self-limiting may be possible for long-pulse ($\tau_p \geq$ 250 ns) YAG lasers at 1064 nm, although we have not tested this possibility.

Acknowledgments

This work was supported at UT by NREL under contract no. ZAF-5-14142-08, which has also supported the contributions of personnel and materials from Solar Cells Inc (Toledo, OH), C J Laser Corp. (Dayton, OH), and ISET (Los Angeles, CA). We are grateful to Bolko von Roedern, our contract monitor, for many helpful suggestions and advice during the course of this contract. To SCI we are grateful for making time available and assisting us in the use of their cwp-Nd:YAG laser and for the many long sessions we have spent behind their Tencor stylus profilometer. Also we appreciate the supply of CIGS-related materials and the very helpful advice we have received from ISET, especially suggestions for interconnect structures to measure series and shunt resistances. We are grateful for the arrangements we could make with the University of Dayton Research Institute (Prof. Alan Lightman) for the use of their Cu-vapor laser, and with Lambda Physik for the use of a KrF laser and beam homogenizer in their applications lab. We are indebted to Spectra Physics for making available to us two diode-laser-pumped Nd:YAG lasers in their applications facility, and to Prof. H.J. Simon for the use of his mode-locked YAG laser at The University of Toledo.

References

[1] J. Wilson and J.F.B. Hawkes, **Lasers: Principles and Applications**, (Prentice Hall, Hertfordshire, UK, 1987) pp. 194ff.

[2] V. Ramanathan, L.A. Russell, C.H. Liu, and P.V. Meyers, "Indoor Stability Tests on CdS/CdTe/ZnTe n-i-p Submodules," Solar Cells **28**, 129-133 (1990).

[3] J.G. O'Dowd, B.J. Johnson, R.S. Oswald, & F. Willing, "The Stability of Laser Weld Interconnects in a-Si:H Modules," Proc. 23rd IEEE PVSC-1993, pp. 926-929; F. Willing, R. Oswald, and J. Newton, "Controlling Shorts in a-Si Modules," Proc. 23rd IEEE PVSC-1993, pp. 946-949.

[4] R. Arya, "Research on Polycrystalline Thin Film Submodules Based on $CuInSe_2$ Materials," Solarex Final Technical Report. NREL contract ZN-1-19019-4 (1995).

[5] S. Nakajima, M. Abe, H. Shinohara, Y. Arai, N. Ishida, A. Satake, K. Nishi, S. Kugawa, Y. Uehara, M. Ishii, & S. Yamazaki, "High Effective Area Amorphous Silicon Solar Cell Using Excimer Laser Process," Proc. 21st IEEE PVSC-1990, 1400 .

[6] P.H. Key, D. Sands, and F.X. Wagner, "UV-Excimer Laser Ablation Patterning of II-VI Compound Semiconductors," Matls. Sci. Forum, 173-174, 59-66 (1995).

[7] L. Quercia, S. Avagliano, A. Parretta, E. Salza, and P. Menna, "Laser Patterning of $CuInSe_2$/Mo/SLS Structures for the Fabrication of CuIn Se_2 Submodules," Matls. Sci. Forum, 173-174, 53-58 (1995).

[8] J.J. Hanak, U.S. Patent No. 4292092 "Laser Processing Technique for Fabricating Series-Connected and Tandem Junction Series-Connected Solar Cells into a Solar Battery," (1981) assigned to RCA Corp., New York, N.Y.

[9] H. Okinawa, K. Nakatani, T. Sato, U.S. Patent No. 4697041 "Integrated Solar Cells," (1987) assigned to Teijin Ltd, Osaka, Jpn;
H. Sinohara, U.S. Patent No. 4861964 "Laser Scriving System and Method," (1989) assigned to Semiconductor Energy Laboratory Co, Ltd, Atsugi, Jpn;
M. Nishiura, T. Ichimura, M. Kamiyama, U.S. Patent No. 4954181 "Solar Cell Module and Method of Manufacture," (1990) assigned to Fuji Electric Co. Ltd, Fuji Electric Corp. Res. & Dev. Ltd, Jpn.
S. Yamazaki, K. Itoh, S. Nagayama, U.S. Patent No. 4970368 "Laser Scribing Method," assigned to Semiconductor Energy Laboratory Co. Ltd., Atsugi, Jpn.
Y. Kaido, O. Masatoshi, U.S. Patent No. 5217921, "Method of Photovoltaic Device Manufacture," (1993), assigned to Sanyo Electric Co, Ltd., Osaka, Jpn.

[10] Solar Cells, Inc., 1700 N. Westwood Ave,Toledo, OH, 43605.

[11] Spectra Physics Inc., 1330 Terra Bella Ave, Mountain View, CA, 94039.

[12] Lambda Physik, 3201 West Commercial Blvd., Ft. Lauderdale, FL, 33309.

[13] Microlas Lasersystem GMBH, Hans-Böckler-Strasse 12, 37079 Gottingen, Germany.

[14] L. Balazs, R. Gijbels, and A. Vertes, "Expansion of Laser-Generated Plumes Near the Plasma Ignition Threshold," Analytical Chemistry **63**, 314 (1991).

[15] R. Srinivasan & V. Mayne-Banton, Appl. Phys. Lett. 41, 576, (1982); J.E. Andrew, P.E. Dyer, D. Forster, and P.H. Key, "Direct Etching of Polymeric Materials Using a XeCl Laser," Appl. Phys. Lett. 43, 717-719 (1983).

[16] *CRC Handbook of Chemistry and Physics*, 78th edition. D.R. Lide, ed. (CRC Press, Boca Raton, 1997).

[17] *Thermal Conductivity, Nonmetallic Solids* and *Specific Heat, Nonmetallic Solids* (vols. 2 & 5 of *Thermophysical Properties of Matter*) edited by Y.S. Touloukian (IFI/Plenum, N.Y. 1970).

Publications

1. A. D. Compaan, "Laser Processing for Thin-Film Photovoltaics," Proc. SPIE 2403, pp. 224-231 (1995).
2. A.D. Compaan, I. Matulionis, M.J. Miller, and U.N. Jayamaha, "Optimization of Laser Scribing for Thin-Film Photovoltaics," 25th IEEE Photovoltaic Specialists Conference-1996, pp. 769-772.
3. A.D. Compaan, Optimization of Laser Scribing for Thin-Film PV Modules, Annual Subcontract Report (4/12/95--4/11/96) Contract No.ZAF-5-14142-08 [available from NTIS].
4. A.D. Compaan, U. Jayamaha, and I. Matulionis, "Optimization of Laser Scribing for Thin-film PV Modules," subcontract report published in: Annual Report, Photovoltaic Subcontract Program, FY 1995, [available from NTIS].
5. A.D. Compaan, I. Matulionis, S. Nakade, and U. Jayamaha, "Pulse Duration and Wavelength Effects in Laser Scribing of Thin-Film Polycrystalline PV Materials," NREL/SNL Photovoltaics Program Review--Proceedings of the 14th Conference, ed. by C.E. Witt, M. Al-Jassim, and J.M. Gee (AIP Conference Proceedings No. 394), (1997), pp. 567-71.
6. A.D. Compaan, U. Jayamaha, I. Matulionis and S. Nakade, "Optimization of Laser Scribing for Thin-film PV Modules," Annual Report, NREL Photovoltaic Program, FY 1996, [to be available from NTIS].
7. I. Matulionis, S. Nakade and A.D. Compaan, "Wavelength and Pulse Duration Effects in Laser Scribing of Thin Films," 26th IEEE Photovoltaic Specialists Conference-1997, pp. 491-494.
8. A.D. Compaan, I. Matulionis and S. Nakade, "Optimization of Laser Scribing for Thin-film PV Modules," subcontract report published in: Annual Report, Photovoltaic Subcontract Program FY 1997, [to be available from NTIS].

Personnel

Postdoctoral associate: Upali Jayamaha 4/95--9/96

Graduate students: Ilvydas Matulionis
M.S. Dec. 1997
Ph.D. in progress
Shogo Nakade
M.S. in progress

REPORT DOCUMENTATION PAGE

Form Approved
OMB NO. 0704-0188

Public reporting burden for this collection of information is estimated to average 1 hour per response, including the time for reviewing instructions, searching existing data sources, gathering and maintaining the data needed, and completing and reviewing the collection of information. Send comments regarding this burden estimate or any other aspect of this collection of information, including suggestions for reducing this burden, to Washington Headquarters Services, Directorate for Information Operations and Reports, 1215 Jefferson Davis Highway, Suite 1204, Arlington, VA 22202-4302, and to the Office of Management and Budget, Paperwork Reduction Project (0704-0188), Washington, DC 20503.

1. AGENCY USE ONLY (Leave blank)	2. REPORT DATE	3. REPORT TYPE AND DATES COVERED
	June 1998	Final Technical Progress Report; 12 April 1995 – 11 October 1997

4. TITLE AND SUBTITLE
Optimization of Laser Scribing for Thin-Film PV Modules, Final Technical Progress Report, 12 April 1995 –11 October 1997

5. FUNDING NUMBERS
C: ZAF-5-14142-08
TA: PV804401

6. AUTHOR(S)
A. D. Compaan, I. Matulionis, and S. Nakade

7. PERFORMING ORGANIZATION NAME(S) AND ADDRESS(ES)
The University of Toledo
2801 W. Bancroft
Toledo, OH 43606

8. PERFORMING ORGANIZATION REPORT NUMBER

9. SPONSORING/MONITORING AGENCY NAME(S) AND ADDRESS(ES)
National Renewable Energy Laboratory
1617 Cole Blvd.
Golden, CO 80401-3393

10. SPONSORING/MONITORING AGENCY REPORT NUMBER
SR-520-24842

11. SUPPLEMENTARY NOTES
NREL Technical Monitor: B. von Roedern

12a. DISTRIBUTION/AVAILABILITY STATEMENT
National Technical Information Service
U.S. Department of Commerce
5285 Port Royal Road
Springfield, VA 22161

12b. DISTRIBUTION CODE

13. ABSTRACT *(Maximum 200 words)*

This report covers the work done by the University of Toledo under this subcontract. Researchers determined the threshold power densities for the onset of ablation from thin films of CdTe, $CuInSe_2$, SnO_2:F, ZnO:Al, gold, and molybdenum for 12 different wavelength laser systems using wide variations of laser pulse durations. Optimum energy density for the most efficient removal of material during scribing strongly depends on the wavelength of the laser and, to a smaller extent, on the pulse duration. The optimum energy densities range from 0.5 J/cm^2 for the 532-nm, 8-nsec YAG pulse on CdTe to 0.2J/cm^2 for the excimer laser at 308 nm on CIS. Poor scribing of CdTe was seen with the 1064-nm beam; ZnO was scribed poorly by all lasers except for the excimer laser. Excellent scribe profiles were observed with the 308-nm excimer lasers on all materials, including ZnO.

14. SUBJECT TERMS
photovoltaics ; thin-film PV modules ; laser scribing ;

15. NUMBER OF PAGES
43

16. PRICE CODE

17. SECURITY CLASSIFICATION OF REPORT	18. SECURITY CLASSIFICATION OF THIS PAGE	19. SECURITY CLASSIFICATION OF ABSTRACT	20. LIMITATION OF ABSTRACT
Unclassified	Unclassified	Unclassified	UL